A novel motif in calcimembrin/C16orf74 dictates multimeric dephosphorylation by calcineurin

Devin A. Bradburn[1,7], Joana C. Reis[2,3,7], R.Yvette Moreno[1], Shariq Qayyum[2,4,5], Thibault Viennet[2,3,6], Haribabu Arthanari[2,3], Martha S. Cyert[1]*

1. Department of Biology, Stanford University, Stanford, CA 94305, USA
2. Department of Cancer Biology, Dana-Farber Cancer Institute, Boston, Massachusetts, USA.
3. Department of Biological Chemistry and Molecular Pharmacology, Harvard Medical School, Boston, Massachusetts, USA.
4. Men's Health: Aging & Metabolism, Brigham and Women's Hospital, Harvard Medical School, Boston, MA, USA.
5. Cardiovascular Research Center, Department of Medicine, Massachusetts General Hospital and Harvard Medical School, Boston, MA, USA
6. Department of Chemistry and iNANO, Aarhus University, Aarhus, Denmark
7. Contributed equally to this work

*Corresponding author:
Department of Biology
410B Bass Biology Building
Stanford University
Stanford, CA 94305-5020
phone: 650 723-9970
fax: 650 724-9945
E-mail: mcyert@stanford.edu

Abstract:

Calcineurin, the Ca^{2+}/calmodulin-activated protein phosphatase, recognizes substrates and regulators via short linear motifs, PxIxIT and LxVP, which dock to distinct sites on calcineurin to determine enzyme distribution and catalysis, respectively. Calcimembrin/C16orf74 (CLMB), an intrinsically disordered microprotein whose expression correlates with poor cancer outcomes, targets calcineurin to membranes where it may promote oncogenesis by shaping calcineurin signaling. We show that CLMB associates with membranes via lipidation, i.e. N-myristoylation and reversible S-acylation. Furthermore, CLMB contains an unusual composite 'LxVPxIxIT' motif, that binds the PxIxIT-docking site on calcineurin with extraordinarily high affinity when phosphorylated, ^{33}LDVPDIIITPP(p)T^{44}. Calcineurin dephosphorylates CLMB to decrease this affinity, but Thr44 is protected from dephosphorylation when PxIxIT-bound. We propose that CLMB is dephosphorylated in multimeric complexes, where one PxIxIT-bound CLMB recruits calcineurin to membranes, allowing a second CLMB to engage via its LxVP motif to be dephosphorylated. *In vivo* and *in vitro* data, including nuclear magnetic resonance (NMR) analyses of CLMB-calcineurin complexes, support this model. Thus, CLMB with its composite motif imposes unique properties to calcineurin signaling at membranes including sensitivity to CLMB:calcineurin ratios, CLMB phosphorylation and dynamic S-acylation.

Introduction

Calcium (Ca^{2+}) ions are spatially and temporally controlled in cells to regulate a wide array of biological processes [1]. Ca^{2+} signaling frequently occurs within membrane-associated microdomains that contain both effector proteins and their substrates. Thus, subcellular localization of calcineurin, the only Ca^{2+}-calmodulin (CaM) regulated serine/threonine protein phosphatase, dictates its signaling specificity[2]. Calcineurin (CNA/B) is an obligate heterodimer composed of catalytic (CNA) and regulatory (CNB) subunits that is activated when Ca^{2+}/calmodulin binding relieves autoinhibition mediated by the CNA C-terminal domain[3]. Calcineurin interacts with partners via two short linear motifs (SLiMs), LxVP and PxIxIT, which cooperate to promote dephosphorylation. PxIxIT binds to CNA independent of $Ca^{2+}$and anchors calcineurin to

substrates and regulators. In contrast, LxVP binds to a site composed of residues in both CNA and CNB and orients substrates for dephosphorylation at a separate catalytic site, marked by Zn^{2+} and Fe^{2+} ions[2, 3]. LxVP binding occurs only after activation by Ca^{2+}/CaM and is blocked by autoinhibitory sequences in CNA as well as the immunosuppressant drugs, Cyclosporin A and FK506[4, 5].

Systematic discovery of PxIxIT and LxVP SLiMs has significantly expanded our knowledge of calcineurin signaling[6, 7, 8, 9] and surprisingly identified at least 31 human proteins that harbor composite calcineurin-binding motifs containing contiguous LxVP and PxIxIT sequences that share a proline (LxVPxIxIT)[9]. Although each SLiM in this composite motif can bind to its cognate site, they are unlikely to do so simultaneously, as their docking surfaces are ~60 Å apart on calcineurin[4, 9]. Thus, how or if these motifs promote dephosphorylation is unclear.

Here we elucidate how C16orf74, a short unstructured microprotein associated with poor outcomes in melanoma, pancreatic and head and neck cancer, is regulated by calcineurin via a composite LxVPxIxIT motif [9, 10]. We name C16orf74 calcimembrin (CLMB), because it associates with membranes via lipidation (N-myristoylation and S-acylation) and recruits calcineurin to these sites. CLMB is phosphorylated at Thr 44 (pThr44) and binds calcineurin with exceptionally high affinity because the flanking LxVP and pThr44 features (LxVPxIxITxx(p)T) enhance PxIxT-mediated binding to CNA. Calcineurin also dephosphorylates pThr44, but this residue is protected when CLMB is bound to the PxIxT-docking surface. Thus, we propose that dephosphorylation occurs in multimers, with one CNA/B bound to two CLMB molecules at the PxIxIT and LxVP-docking sites, respectively. NMR confirms formation of these complexes *in vitro*. Furthermore, this multimeric model predicts that CLMB dephosphorylation varies depending on the amount of CLMB relative to calcineurin, which we demonstrate via in cell analyses and kinetic modeling of dephosphorylation *in vitro*. In summary, this work reveals how CLMB can dynamically shape calcineurin signaling through a mechanism dictated by its composite motif and reversible association with membranes.

53 **Results**

54 **Calcimembrin is myristoylated and S-acylated.** CLMB lacks predicted transmembrane domains but may
55 associate with membranes via lipidation (Fig. 1a)[10]. CLMB contains a glycine at position 2 (Gly2), a site
56 frequently modified by myristate, a 14-carbon lipid whose co-translational addition can promote protein
57 association with membranes[11]. CLMB also has two cysteines near in its N-terminus, Cys7 and Cys14, one
58 of which, Cys7, is predicted to be modified by S-acylation, the reversible addition of a fatty acid, usually a
59 16-carbon palmitate, that regulates membrane localization[12]. To determine if CLMB is lipidated, we
60 metabolically labeled HEK293 Flp-In T-REx cells inducibly expressing wildtype CLMB-FLAG ($CLMB_{WT}$)
61 with YnMyr and 17-ODYA, alkyne-containing analogs of myristate and palmitate respectively[13]. Following
62 immunoprecipitation, analog incorporation was detected via addition of biotin using CLICK-chemistry
63 followed by visualization with streptavidin (Fig. 1b). $CLMB_{WT}$ incorporated YnMyr and 17-ODYA,
64 indicating that the protein is both myristoylated and palmitoylated. To identify which residues were
65 lipidated, we mutated proposed sites of S-acylation ($CLMB_{C7,14S}$), and myristoylation ($CLMB_{G2A}$ (Fig. 1b).
66 The mutants were expressed at low levels suggesting instability, which we countered by including a
67 proteasome inhibitor (MG132) in the analyses. $CLMB_{C7,14S}$ showed no 17-ODYA incorporation but
68 maintained YnMyr suggesting that Cys7 and/or Cys14 are S-acylated. By contrast, neither lipid
69 modification was detected for $CLMB_{G2A}$, which confirms that Gly2 is myristoylated. Because
70 myristoylation can promote S-acylation by anchoring a protein to the membrane[14], we then examined
71 $CLMB_{G2A}$ for S-acylation with increased sensitivity by including palmostatin B (PalmB), a pan-inhibitor
72 of thioesterases that remove S-acylation[15]. In the presence of this inhibitor, 17-ODYA incorporation into
73 both $CLMB_{WT}$ and $CLMB_{G2A}$ was observed (Supplementary Fig.1), indicating that $CLMB_{G2A}$ is S-acylated,
74 but with reduced efficiency.

75 To determine if CLMB-FLAG is dually S-acylated at Cys7 and Cys14, we used acyl-PEG exchange (APE)
76 in which S-acylated groups are cleaved using hydroxylamine (NH_2OH) and exchanged for a PEGylated
77 molecule that increases protein mass by 5 kDa for each S-acylated residue[16] (Fig.1c). Endogenous calnexin,

78 a dually acylated protein, served as a positive control for each sample. For $CLMB_{WT}$, two slower migrating
79 bands were observed. $CLMB_{C7S}$ lacked the upper band, while $CLMB_{C7,14S}$ was unmodified, indicating that
80 Cys7 and Cys14 are S-acylated in $CLMB_{WT}$ (Fig. 1c). $CLMB_{G2A}$ displayed two sites of S-acylation, but
81 with reduced intensity relative to $CLMB_{WT}$, consistent with results from metabolic labeling (Fig. 1b).
82 Together these findings establish that CLMB is myristoylated at Gly2 and S-acylated at Cys7 and Cys14.

83 **Dynamic S-acylation of CLMB mediates membrane association.** To examine whether S-acylation of
84 CLMB is dynamic[17], we carried out a pair of pulse-chase analyses with two metabolic labels (Fig. 1d, e).
85 L-AHA, an azide-containing methionine analog detected CLMB-FLAG protein levels, while in parallel,
86 17-ODYA detected S-acylation. CLMB-FLAG was immunopurified (IP) after labeling for one hour
87 followed by a 30-minute chase with DMSO or PalmB. Quantifying the 17-ODYA to L-AHA ratio revealed
88 that palmitate incorporation into CLMB increased ~3-fold when thioesterases were inhibited (Fig, 1e,
89 PalmB vs DMSO). This indicates that S-acylation of CLMB turns over rapidly relative to its rate of
90 degradation.

91 To determine if lipidation mediates CLMB membrane recruitment, we analyzed the localization of
92 $CLMB_{WT}$ and lipidation defective mutants, $CLMB_{G2A}$ and $CLMB_{C7,14S}$. Detergent-assisted subcellular
93 fractionation showed that $CLMB_{WT}$ was primarily membrane associated, appearing in fractions marked by
94 GM130, a Golgi protein. By contrast, both mutants were predominantly cytosolic, appearing in fractions
95 marked by α-tubulin (Fig. 1 f, g). Together these analyses indicate that N-myristoylation, in combination
96 with dynamic dual S-acylation, promote the stable association of CLMB with membranes.

97 **The composite SLiM in CLMB mediates binding to and dephosphorylation by calcineurin.** Next, we
98 examined how each part of CLMB's composite motif, LDVPDIIIT, contributes to calcineurin binding by
99 generating mutants, $CLMB_{IxITMut}$ (LDVPD**AIAA**) and $CLMB_{LxVMut}$, (**A**D**A**PDIIIT) (Fig. 1a) that disrupt
100 each motif independently without altering the shared proline. To examine binding of these mutants to
101 calcineurin, the association of CLMB-FLAG with GFP-tagged calcineurin (CNA-GFP complexed with

102 endogenous CNB) was assessed following purification of calcineurin from lysates of HEK293 cells co-
103 transfected with these constructs (Fig. 2a, b). $CLMB_{WT}$ but not $CLMB_{IxITMut}$ co-purified with calcineurin,
104 showing that this interaction was PxIxIT-dependent. Less calcineurin co-purified with $CLMB_{LxVMut}$ vs.
105 $CLMB_{WT}$, showing that the LxVP also makes a modest contribution to calcineurin binding. Furthermore,
106 when expressed and analyzed by SDS-polyacrylamide gel electrophoresis (SDS-PAGE), both mutants
107 displayed two electrophoretic forms, with a slower migrating band also faintly observed for $CLMB_{WT}$ (Fig.
108 2a, input). Phosphorylation, which often reduces electrophoretic mobility, has been reported for CLMB at
109 Thr44 (pThr44) and less frequently at Thr46[18]. We confirmed that the slower migrating forms of CLMB
110 contained pThr44, as they were absent in mutants lacking this residue ($CLMB_{T44A}$, $CLMB_{T44A+LxVMut}$,
111 $CLMB_{T44A,T46A}$), but not in $CLMB_{T46A}$ (Fig. 2a, Supplemental Fig. 2a). These observations indicate that
112 calcineurin binds to CLMB and dephosphorylates pThr44, which is disrupted when either the LxVP or
113 PxIxIT portion of the composite motif is compromised.

114 Finally, we confirmed that pThr44 enhance binding to calcineurin, as the slower migrating (phosphorylated)
115 forms of $CLMB_{WT}$ and $CLMB_{LxVMut}$ predominantly co-purified with calcineurin (Fig. 2a, IP)[10]. Indeed,
116 $CLMB_{T44A}$ displayed reduced binding to calcineurin, which was further reduced by mutating LxV
117 ($CLMB_{T44A+LxVMut}$) (Fig. 2a, b).

118 The contributions of PxIxIT, LxVP, and pThr44 to calcineurin binding were also examined by measuring
119 the extent of CLMB co-localization with calcineurin (CNA-GFP complexed with endogenous CNB) via
120 immunofluorescence (IF) (Fig. 2c, d). When co-transfected into MCF7 cells $CLMB_{WT}$-FLAG and
121 calcineurin colocalize at membranes (see regions marked by arrows in Fig. 2c). In contrast, when co-
122 expressed with $CLMB_{IxITMut}$, this colocalization was greatly reduced and calcineurin was predominantly
123 cytosolic. $CLMB_{LxVMut}$ and $CLMB_{T44A}$ also displayed reduced colocalization with calcineurin (Fig. 2c, d),
124 mirroring the trends observed in co-purification analyses (Fig. 2a, b). Thus, CLMB recruits calcineurin to
125 membranes primarily via PxIxT-mediated binding.

126 Finally, dephosphorylation of pThr44 in CLMB by calcineurin was demonstrated *in vitro* using
127 phosphorylated peptide substrates that encode residues 21-50 (Fig. 1a). The peptide from $pCLMB_{WT}$ was
128 robustly dephosphorylated compared to $pCLMB_{LxVMut}$ (Fig. 2e) showing that, as for other calcineurin
129 substrates, the LxVP motif promotes catalysis[19]. Finally, the presence of a functional LxVP motif in the
130 $CLMB_{WT}$ peptide was also confirmed by its ability to inhibit dephosphorylation of the RII peptide, an
131 LxVP-containing calcineurin substrate derived from the regulatory subunit of protein kinase A (RII
132 isoform)[19] (Supplemental Fig. 2b). Together, these data show that both the LxVP and PxIxIT components
133 of the composite motif are functional, that CLMB is a calcineurin substrate, and that pThr44 increases
134 CLMB binding to calcineurin.

135 **Phosphorylated Thr44 and the LxVP motif enhance CLMB binding to the PxIxIT docking site.** To
136 quantitatively assess CLMB-calcineurin interaction, we used isothermal titration calorimetry (ITC) and
137 fluorescence polarization anisotropy (FP) to measure binding of CLMB peptides containing the composite
138 SLiM (residues 21-50) to purified, catalytically inactive CNA/B containing $CNA_{Trunc+H151Q}$. This mutant
139 CNA lacks the C-terminal autoinhibitory region, which allows LxVP motifs to bind to CNA/B in the
140 absence of Ca^{2+}/CaM[20]. ITC revealed that the phosphorylated $CLMB_{WT}$ peptide ($pCLMB_{WT}$) binds
141 calcineurin at a one-to-one ratio with high affinity (K_D= 37 nM), (Fig. 3a). FP using FITC-labelled peptides
142 at pH 7.4 revealed that phosphorylation of Thr44 enhances CLMB binding to calcineurin ~20-fold (K_D =
143 14.1 nM vs 291 nM) (Fig. 3b). Furthermore, the affinity of $pCLMB_{WT}$ for calcineurin was similar over a
144 pH range (6.9-8.0) which should change the protonation state of histidine residues (Supplemental Fig. 3a,
145 b). This included the histidine immediately preceding the LxVP (H32) which is expected to engage with
146 calcineurin during LxVP docking[7]. The concordance between measurements made with CLMB peptide that
147 is tag-free (ITC) vs. tagged with fluorescein isothiocyanate (FITC) (FP) (37 vs 14.1 nM for $pCLMB_{WT}$)
148 (Fig. 3a, b), shows that the tag does not significantly affect binding affinity. Given the high-throughput
149 capability of FP, this method was used for the remaining comparisons. To test if the high affinity $pCLMB_{WT}$-
150 calcineurin binding observed was PxIxIT-mediated, we used FP to assess the ability of CLMB peptides to

151 compete with a well characterized PxIxIT peptide, FITC-PVIVIT [21, 22], for calcineurin binding (Fig. 3c, e).
152 $pCLMB_{WT}$ competed with PVIVIT most effectively, with peptides lacking the LxVP motif ($pCLMB_{LxVMut}$),
153 or pThr44 ($CLMB_{WT}$) showing reduced competition (Fig. 3c, e). $pCLMB_{IxITMut}$ lacking the PxIxIT motif
154 was unable to displace PVIVIT from CNA/B. When these experiments were repeated using FITC-
155 $pCLMB_{WT}$ peptide in place of FITC-PVIVIT (Fig. 3d, e), a similar pattern was observed, although
156 phosphorylation of T44 ($pCLMB_{WT}$ vs $CLMB_{WT}$) caused a much greater reduction in Ki (30X vs 3X for
157 PVIVIT competition). Importantly, CLMB peptides accurately mimic full length CLMB binding to
158 calcineurin as both caused equivalent displacement of FITC-$pCLMB_{WT}$ (Supplemental Fig. 3c,d).
159 Altogether, these data show that, like PVIVIT, $pCLMB_{WT}$ peptides bind to the PxIxIT docking groove on
160 CNA and that flanking residues, i.e. LxV and pThr44, enhance binding to form an extended
161 LxVPxIxITxxT(p) sequence with exceptionally high affinity for calcineurin.

162 **NMR analysis shows CLMB binding to two sites on calcineurin.** Next, to investigate the structure of
163 CLMB in the presence and absence of calcineurin, we used solution-state NMR. 88% of non-proline
164 backbone resonances were assigned using a standard set of triple-resonance experiments, utilizing full-
165 length dually ^{13}C- and ^{15}N-labeled CLMB (76 residues) that was expressed in *E.coli* (Fig. 4a, Supplemental
166 Fig. 4a). To assess CLMB secondary structure, we employed TALOS-N, a computational method that
167 predicts backbone torsion angles from NMR chemical shifts[23]. This revealed that CLMB is disordered
168 overall, but contains two regions with a tendency to form a β-strand (Supplemental Fig. 4b): Residues I38-
169 I40 include the PxIxIT, consistent with binding of this motif-type to CNA as a β-strand [22]. N-terminal
170 residues, Q12-V15, were also predisposed to localized folding suggesting possible involvement in other
171 binding interactions. Similar analyses carried out for CLMB using chemical shift secondary structure
172 population interference (CheSPI)[24] confirmed the absence of secondary structure (Supplemental Fig. 4c).

173 To map the interaction interface of calcineurin on CLMB, we focused first on PxIxIT-mediated interactions
174 by titrating ^{15}N-labeled CLMB with varying molar ratios of monomeric recombinant CNA in the absence
175 of CNB and monitoring the interaction through ^{15}N-^{1}H SOFAST-HMQC experiments (Fig.4). No additional

176 insights were gained from BEST-TROSY experiments[25]. CNA can bind to PxIxIT motifs but lacks the LxVP
177 binding surface found at the interface of CNA and CNB[4]. Due to the size of the CLMB-CNA complex, we
178 anticipated significant broadening of NMR signals at the interaction interface. This broadening can also
179 arise from exchange kinetics between the observable CLMB and the titrant, CNA, making it challenging to
180 distinguish the two effects. As expected, at a molar ratio of 2:1 (CLMB: CNA), many of the CLMB signals
181 undergo significant line broadening (Fig.4b), which become more pronounced at a molar ratio to 1:1, due
182 to the majority of CLMB being bound to CNA (Fig.4c). This is particularly true for signals corresponding
183 to the PxIxIT and LxVP motifs, indicating, as observed in FP experiments, that LxV residues participate in
184 binding to the PxIxIT interface (Fig. 4b, c, Supplemental Fig. 2d). Line broadening across the majority of
185 CLMB residues indicates that the interaction interface on CLMB extends beyond the PxIxIT and LxVP
186 motifs (Fig.4 b, c). Interactions with the N- and C-terminal residues of CLMB may be an avidity-driven
187 effect, anchored by PxIxIT binding, as has been reported for other calcineurin substrates [26].

188 To investigate binding that may occur at the LxVP docking site of calcineurin, we next titrated CLMB with
189 the heterodimeric CNA/B complex (Fig.4d, e). Signal broadening at the N-terminus of CLMB was more
190 pronounced with CNA/B relative to CNA alone, suggesting possible interactions between CLMB and CNB
191 (Fig. 4b, c vs 4d, e, and Supplemental Fig. 4d). These include the Q9-V12 region that displayed partial
192 folding in the absence of calcineurin. At a molar ratio of 2:1 (CLMB: CNA/B), more broadening is observed
193 in LxVP but not PxIxIT residues when compared to the interaction with CNA (Fig. 4d vs 4b, and
194 Supplemental Fig. 4c). This includes not only L33 and V35, but also H32, another residue expected to
195 participate in LxVP binding to CNA/B[7]. However, at a molar ratio of 1:1, where essentially all CLMB
196 should be PxIxIT-bound (given the higher K_D for PxIxIT vs LxVP and our working concentrations), the
197 pattern of line broadening at the composite motif is similar when complexed with either CNA or CNA/B
198 (Fig. 4c vs 4e). To better visualize LxVP-mediated binding of CLMB to CNA/B, NMR analyses were also
199 performed in the presence of $pCLMB_{LxVPmut}$ peptide (which was not isotopically labeled) to saturate the
200 PxIxIT binding site on CNA/B (Supplemental Fig. 5). While addition of this peptide on its own caused no

201 change in the NMR spectrum for ^{15}N-labeled CLMB (Supplemental Fig. 5a), in the presence of CNA/B
202 (2:1 or 1:1 CLMB: CNA) residues in the LxVP motif, particularly H32 and L33, displayed shifting and
203 broadening effects in addition to N-terminal residues, as previously observed (Supplemental Fig. 5b,c).
204 Together these findings show that when in excess (2 CLMB: 1 CNA/B), CLMB engages calcineurin
205 (CNA/B) through both its LxVP and PxIxIT motifs.

206 To investigate the CLMB-calcineurin interaction further, we carried out structural predictions using
207 AlphaFold 3 for 2 CLMB molecules and CNA/B containing truncated CNA lacking the C-terminal
208 calmodulin binding and regulatory domains (Supplemental Fig. 6a-c) [27]. Consistent with our NMR analyses,
209 the models show two copies of CLMB simultaneously bound to CNA/B, one each at the LxVP and PxIxIT
210 docking sites. Predicted interactions of pCLMB containing pThr44 with CNA/B was nearly identical,
211 however with the LxVP-bound CLMB molecule showing an additional interaction of pThr44 with the
212 active site, as would occur during catalysis (Supplemental Fig. 6a-c). Thus, these models suggest that
213 formation of multimeric complexes (2 CLMB: 1 CNA/B) will facilitate dephosphorylation of pCLMB.

214 **Calcineurin dephosphorylates CLMB by forming multimers.** Next, we sought to test the prediction that
215 pThr44 dephosphorylation is promoted when CLMB is in excess (2 CLMB: 1 CNA/B) but inhibited at
216 lower CLMB: CNA/B ratios where PxIxIT-bound complexes are favored and protect pThr44 from
217 dephosphorylation. To this end, we inducibly expressed $CLMB_{WT}$-FLAG in HEK293 Flp-In T-REx cells
218 and compared its phosphorylation status with endogenous vs overexpressed calcineurin (i.e. transfection of
219 GFP-CNA, which complexes with endogenous CNB). In stark contrast to a typical substrate, CLMB-FLAG
220 phosphorylation at T44 increased upon calcineurin overexpression (Fig. 5a,b, Supplemental Fig.7a). Intact
221 PxIxIT binding rather than catalytic activity was required for this effect, as overexpressing catalytically
222 inactive calcineurin (containing GFP-CNA_{H151Q}) [28], but not calcineurin that is defective for PxIxIT binding
223 (containing GFP-CNA_{NIR}) [29], increased CLMB-FLAG phosphorylation (Supplemental Fig. 7b). We
224 predicted that further increasing CLMB levels in these calcineurin overexpressing cells would promote
225 dephosphorylation of CLMB-FLAG by increasing the CLMB:CNA/B ratio. Thus, we overexpressed V5-

226 tagged CLMB in HEK293 Flp-In T-REx cells that inducibly expressed CLMB-FLAG and overexpressed
227 calcineurin (GFP-CNA complexed with endogenous CNB) (Fig. 5a-c). As predicted, phosphorylation of
228 $CLMB_{WT}$-FLAG decreased upon expression of $CLMB_{WT}$-V5. This effect was dependent on PxIxIT binding,
229 as introducing $CLMB_{IxITMut}$-V5 did not decrease $CLMB_{WT}$-FLAG phosphorylation, but $CLMB_{LxVMut}$-V5,
230 which contains an intact PxIxIT motif, did (Fig, 5a-c). for $CLMB_{WT}$, when $CLMB_{LxVMut}$ was expressed,
231 its phosphorylation was enhanced by overexpression of calcineurin and rescued by co-expression of
232 $CLMB_{WT}$-V5 or $CLMB_{LxVMut}$-V5 but not $CLMB_{IxITMut}$-V5. However, because dephosphorylation is
233 impaired by mutation of the LxV (Fig. 2e), $CLMB_{LxV}$-FLAG displayed increased levels of phosphorylation
234 relative to $CLMB_{WT}$ under all conditions (Fig.5a, b). Finally, we repeated these analyses using $CLMB_{IxITMut}$-
235 FLAG, which displayed partial phosphorylation regardless of calcineurin levels. Surprisingly, $CLMB_{IxITMut}$-
236 FLAG was predominantly dephosphorylated when co-expressed with $CLMB_{WT}$-V5 or $CLMB_{LxVMut}$-V5 but
237 not $CLMB_{IxITMut}$-V5 (Fig. 5a, b). Thus, although the LxVP and PxIxIT components of the CLMB composite
238 motif are both required for efficient dephosphorylation, they do not need to be on the same molecule. A
239 single copy of CLMB must have an LxVP to mediate its own dephosphorylation but can utilize the PxIxIT
240 of neighboring copies to recruit calcineurin, promote LxVP binding, and be dephosphorylated (Fig. 5c,
241 bottom row).
242 To demonstrate more precisely how the ratio of CLMB to calcineurin affects dephosphorylation, we
243 conducted a series of *in vitro* dephosphorylation assays using a fixed substrate concentration (100nM
244 $pCLMB_{WT}$ or $pCLMB_{IxITMut}$ peptides) with increasing concentrations of purified calcineurin (CNA/B) (20,
245 100 or 200nM) (Fig. 5d, top row). Under these *in vitro* conditions, $pCLMB_{IxITMut}$ was efficiently
246 dephosphorylated due to high enzyme and substrate concentrations and the absence of any competing
247 PxIxIT-containing proteins. For $pCLMB_{IxITMut}$, we observed that dephosphorylation rates increased
248 significantly with the calcineurin concentration (Fig. 5d, top row). In contrast, dephosphorylation of
249 $pCLMB_{WT}$ increased modestly as calcineurin increased from 20 vs 100 nM, and then decreased slightly at
250 200nM calcineurin, where enzyme concentration exceeded that of substrate (100 nM) (Fig. 5d, top row).
251 To better understand this unusual reaction behavior, we turned to kinetic modeling. First, we developed a

252 model describing the complex series of reactions we expect to occur, based on our NMR and in cell analyses
253 of CLMB-calcineurin interactions (Supplemental Fig. 8). For $pCLMB_{IxITMut}$, which contains only an LxVP
254 motif (Supplemental Fig. 8b), substrate binds to the LxVP-docking site of calcineurin (k_2, k_{-2}) and is
255 dephosphorylated (k_3) leading to product formation. Thus, dephosphorylation accelerates with increasing
256 enzyme concentration (Fig. 5d, top row). However, for dephosphorylation of $pCLMB_{WT}$ (Supplemental Fig
257 8a), we propose competition between two binding modes: high affinity binding to the PxIxIT-docking site
258 (k_1, k_{-1}), which prevents pT44 phosphorylation, or lower affinity LxVP-mediated binding (k_2, k_{-2}), which
259 leads to dephosphorylation (k_3). Furthermore, the model allows one enzyme molecule to bind substrate at
260 each of these sites simultaneously (ES1S2). For this complex reaction mechanism, increasing enzyme
261 concentration drives formation of more LxVP-bound substrate and dephosphorylation, but this is offset by
262 reduced substrate availability due to increased PxIxIT-mediated substrate binding and pThr44 protection.
263 Thus, dephosphorylation rates decrease as enzyme concentration exceeds that of substrate (Fig. 5d, top
264 row).

265 To further probe this proposed mechanism, we then used kinetic modeling software (KintekExploer™)
266 which fits experimental data directly through dynamic simulation and does not require simplifying
267 assumptions[30]. After providing initial values for rate constants consistent with published reports[6, 31], our
268 experimental data were fit to the proposed kinetic model (Fig. 5d bottom row and Supplemental Fig. 8).
269 The resulting rate parameters were well within expected values, and the predicted K_D for phosphorylated
270 PxIxIT binding to calcineurin was 7nM (Supplemental Fig. 8c), which agrees well with experimentally
271 determined values (Fig. 3a, c). However, we noted that some parameters, particularly on and off rates for
272 substrate binding were poorly constrained by the model. Therefore, we manually manipulated different
273 parameters to better understand how relationships between them influenced the fit to our data
274 (Supplemental Fig. 9). This revealed that the equilibrium binding constant for phospho-PxIxIT binding was
275 critical rather than specific on and off rates (k_1 and k_{-1}) (Supplemental Fig. 9a and b). Furthermore, the k_1
276 and k_{-1} values predicted by kinetic simulations represented lower limits for these rates as decreasing them

277 caused significant deviations from the data despite keeping the K_D constant (Supplemental Fig. 9b).
278 Similarly, k_{off} for LxVP binding (k_{-2}) and k_{cat} (k_3) could be increased proportionally without significantly
279 affecting the overall fit (Supplemental Fig. 9c), suggesting that the catalytic efficiency of LxVP-mediated
280 dephosphorylation is a key driver of the observed reaction kinetics. Confirming this, we found that
281 maintaining the second order rate constant was critical for good agreement between the data and the model
282 (Supplemental Fig. 9d). Thus overall, kinetic modeling of our *in vitro* dephosphorylation data supports the
283 hypothesis that phosphorylated CLMB is dephosphorylated via multimer formation. This novel mechanism,
284 which requires substrate levels to exceed that of calcineurin for efficient dephosphorylation, is dictated by
285 the composite LxVPxIxIT motif.

286

287 **Discussion**

288 Here we describe multivalent interactions between calcineurin and CLMB, an intrinsically disordered
289 microprotein and calcineurin substrate that dynamically associates with membranes via protein lipidation.
290 We elucidate roles for a novel composite motif in CLMB, LxVPxIxIT, that combines two SLiMs, PxIxIT
291 and LxVP, with distinct binding modes and functions in calcineurin signaling.

292 Calcineurin, the conserved and ubiquitously expressed calcium/calmodulin regulated protein phosphatase,
293 has been categorized as a dynamic or date hub and specifically as a linear motif binding hub (LMB-hub)
294 because it engages a diverse set of partners that bind competitively to the structurally plastic PxIxIT docking
295 groove[32]. PxIxIT peptides from natural substrates bind to calcineurin as a β strand, vary greatly in sequence
296 and typically have low affinities (~2.5 to 250 micomolar)[26, 33], while regulators and scaffolds, including
297 PVIVIT, the selected inhibitor peptide, have K_D's of ~0.5 micromolar [21, 34, 35]. By contrast, we show that
298 the ^{32}HLDVPDIIITPP(p)TP^{45} sequence in CLMB binds calcineurin at the PxIxIT-docking groove with a
299 K_D of ~14 nM. This extraordinary affinity is mediated predominantly via binding of the core PxIxIT motif
300 which is enhanced ~20 fold by phosphorylation at the +3 position (pThr44), and ~5 fold by the N-terminal
301 LxV sequence (Fig. 3). Such high affinities have also been achieved by engineering the PVIVIT peptide to

302 include a hydrophobic residue at the -1 position and a phosphothreonine at the +3 position, although
303 phosphorylation does not universally enhance PxIxIT affinity[35]. A natural PxIxIT peptide derived from an
304 endogenous inhibitor of calcineurin (CABIN1),[2145]PPEITVTPP(p)TP[2156] also shows high affinity (~170
305 nM) due to phosphorylation of its C-terminal sequence, PPTP, which is identical to that found in CLMB[34].
306 This proline-rich sequence is predicted to form a polyproline helix that may function to extend the β-strand
307 interaction with calcineurin[36, 37]. Thus, the composite LxVPxIxIT motif in CLMB combines several features
308 that consistently stabilize PxIxT-docking. Because calcineurin is an LMB-hub, such high affinity PxIxIT
309 peptides typically inhibit signaling by preventing its interaction with substrates[35, 38]. It is surprising,
310 therefore that CLMB exhibits high affinity PxIxIT-mediated docking yet is also dephosphorylated by
311 calcineurin. As we demonstrate, this is only possible due to the LxVP portion of the composite SLiM in
312 CLMB, and dephosphorylation can only occur when excess CLMB levels allow lower affinity LxVP-
313 docking to occur on a molecule of calcineurin whose PxIxIT-docking site is saturated.

314 Based on our findings, we present two models for how CLMB may shape calcineurin activity *in vivo* (Figure
315 6). First, dynamic S-acylation promotes CLMB association with membranes (Fig. 6a, Step 1), where, when
316 phosphorylated, it recruits a localized pool of calcineurin via high affinity PxIxIT-mediated binding, (Fig.
317 6a, Step 2). This membrane sequestration may prevent calcineurin from dephosphorylating substrates in
318 other cellular locations. In the presence of a Ca^{2+} signal, Ca^{2+} and CaM then activate calcineurin, which
319 exposes the LxVP docking site[39]. If CLMB is in excess relative to calcineurin and PxIxIT binding is fully
320 saturated, a second CLMB molecule will bind via its LxVP motif which positions pThr44 for
321 dephosphorylation at the active site (Fig. 6a, Step 3). However, as the population of CLMB shifts to the
322 dephosphorylated form, PxIxIT binding affinity decreases (Fig. 3) which promotes calcineurin dissociation
323 from CLMB, allowing the enzyme to engage and dephosphorylate other nearby LxVP- and PxIxIT-
324 containing substrates (Fig. 6a, Step 4). This tuning of PxIxIT affinity is critical for signaling as demonstrated
325 for AKAP5, a scaffold that concentrates both calcineurin and NFAT near L-type Ca^{2+} channels in neurons

326 to promote NFAT dephosphorylation[40]. In that case, increasing the AKAP5 PxIxIT affinity for calcineurin
327 ~two-fold significantly impaired NFAT activation due to increased sequestering of calcineurin[41].

328 In our second model (Fig. 6b), active calcineurin-pCLMB dimers (1 CLMB: 1 CNA/B) directly engage and
329 dephosphorylate substrates at the membrane that contain an LxVP, but no PxIxIT motif (Fig. 6b, step 3).
330 Such substrates are exemplified by PRKAR2A, the type II-alpha regulatory subunit of protein kinase A,
331 which contains an LxVP but depends on the PxIxIT motif within its binding partner, AKAP5, to recruit
332 calcineurin and promote dephosphorylation[9, 42]. Proteome-wide predictions suggest that many proteins may
333 similarly harbor an LxVP without an associated PxIxIT [9]. In our second model (Fig. 6b), active calcineurin-
334 pCLMB dimers (1 CLMB: 1 CNA/B) directly engage and dephosphorylate such PxIxIT-less substrates at
335 the membrane (Fig. 6b, step 3). Simply recruiting calcineurin to membranes, where association kinetics are
336 20-30 fold faster than in the cytosol of eukaryotic cells, may enhance LxVP binding causing their efficient
337 dephosphorylation in the absence of a PxIxIT motif [43]. Such division of the PxIxIT and LxVP motifs among
338 two molecules may also allow for the extremely high affinity PxIxIT observed in CLMB. In substrates that
339 contain both a LxVP and PxIxIT motif, stable PxIxIT binding would be expected to limit enzymatic
340 efficiency by slowing product release. However, acting only as a scaffold, CLMB can remain tightly
341 associated with calcineurin via PxIxIT-binding while other substrates cycle in and out of the LxVP-binding
342 surface to be dephosphorylated. In this scenario (Fig. 6b), calcineurin remains at the membrane either until
343 CLMB levels increase sufficiently to allow CLMB dephosphorylation and calcineurin dissociation (Fig. 6b
344 step 4) or until CLMB is de-acylated. In both models, intracellular Ca^{2+} dynamics, CLMB protein levels,
345 and S-acylation/de-acylation activities combine to modulate calcineurin signaling. Future studies aim to
346 identify the palmitoyl acyltransferases (PATs) and acyl protein thioesterases (APTs) that dynamically
347 regulate CLMB S-acylation to better understand how these critical regulators contribute to calcineurin-
348 CLMB signaling *in vivo*.

349 Another missing player in our model is the kinase(s) that phosphorylates CLMB at Thr44. One candidate
350 is the stress-activated p38 mitogen-activated protein kinase (MAPK), which phosphorylates the identical

351 PxIxIT-flanking sequence in Cabin1 (PP(p)TP)[44]. Because phosphorylation increases CLMB-calcineurin
352 affinity, kinase activation is required to prime regulation of calcineurin signaling by CLMB. However,
353 phosphorylation also establishes a negative feedback mechanism, with dephosphorylation decreasing
354 calcineurin's interaction with its substrate. Thus, regulators that modify kinase activity may also
355 significantly affect CLMB-calcineurin signaling dynamics.

356 This study highlights the critical role that SLiMs play in conferring flexibility, tunability and dynamism to
357 cell signaling at the molecular level. Further studies are needed to establish whether composite LxVPxIxT
358 motifs always limit substrate dephosphorylation to occurring in a multimeric complex. Of at least 30 human
359 proteins containing predicted LxVPxIxIT motifs, several are ion channels, such as TRPM6, that assemble
360 into higher order complexes[45], suggesting that these motifs could be a fidelity mechanism that limits
361 dephosphorylation to substrates that are properly assembled into complexes. Similarly, multivalency is a
362 characteristic exhibited by many SLiMs. Some composite SLiMs bind multiple partners in an exclusive
363 manner, for example requiring a kinase and a phosphatase to compete for access to a shared substrate[46, 47].
364 For the intermediate chain of dynein, multivalency regulates assembly of the dynein complex and its
365 interaction with distinct binding partners[48]. In the cell cycle regulator CDKN1A (p21), sequences that flank
366 the PCNA-binding SLiM also encode an essential nuclear localization sequence[49]. Thus, 'composite' SLiMs
367 that encode multiple interactions may be more common that currently appreciated. This complexity
368 emphasizes how critical SLiM-based interactions are for integrating and coordinating the plethora of
369 possible protein-protein interactions that dictate cellular responses.

370 A major challenge that lies ahead is to identify the molecular targets and physiological functions that are
371 regulated by calcineurin-CLMB. While this manuscript was being revised for publication, another study
372 showed that C16orf74/MICT1 is highly expressed in brown fat in mice and controls thermogenesis by
373 regulating the dephosphorylation of PKA RIIβ by calcineurin[50]. In some pancreatic ductal adenocarcinoma
374 (PDAC) derived cell lines, CLMB increases proliferation and migration suggesting that CLMB shapes
375 calcineurin signaling to promote oncogenesis[10]. Indeed, high CLMB expression is associated with poor

376 patient outcomes for PDAC, melanoma and head and neck cancer[10, 51]. Mechanisms underlying these
377 activities have not yet been identified, but these cancers may provide good starting points for examining
378 how CLMB modifies calcineurin signaling in a clinically relevant context.
379
380 **Methods**
381 **Cell culture and transfection:**
382 Cells were cultured at 37 °C in 5% CO_2. HEK293 Flp-In TReX and MCF7 cell lines were grown in standard
383 media containing Dulbecco's modified eagle's medium (DMEM) with 4.5 mg/mL glucose, L-glutamine,
384 and sodium pyruvate (Cytiva SH30243.FS) supplemented with 10% fetal bovine serum (Corning
385 MT35010CV). Transfections were done according to manufacturer instructions. HEK293 cells were
386 transfected using lipofectamine 2000 (Thermo Fisher Scientific 11668019). MCF7 cells were transfected
387 using Transfex ATCC transfection reagent (ATCC ACS-4005).
388
389 **Stable cell line generation:**
390 On day one, 9.6 x 10^5 HEK293 Flp-In TReX cells were transfected using lipofectamine 2000 with 1.5 µg
391 pOG44 and 0. 5 µg pcDNA5 FRT TO encoding proteins of interest in a 6 well dish (plasmid # 2801, 2852,
392 2860, 2861, 2862, 2863, 2864, and 2880). Transfections were done according to manufacturer instructions.
393 On day two, transfected cells were passaged onto 10cm plates. On day three, selection was started using
394 media containing 3 µg blasticidin and 200 ng/mL hygromycin. Selection media was replaced every 2-3
395 days until distinct colonies appeared. Colonies were selected using cloning rings and expanded before being
396 stored in liquid nitrogen.
397
398 **Metabolic labeling to detect CLMB lipidation:**
399 HEK293 Flp-In TReX lines stably expressing $CLMB_{WT}$, $CLMB_{C7,14S}$, or $CLMB_{G2A}$ were induced with 10
400 ng/mL doxycycline for 24 hours and split evenly among three 10 cm tissue culture dishes. The following
401 day, cells were rinsed with PBS and incubated in DMEM containing 4.5 mg/mL glucose, L-glutamine,

402 sodium pyruvate, 2% FBS, and either 20 μM YnMyr (Click Chemistry Tools 1164-5), 30 μM 17-ODYA
403 (Cayman Chemical Company 34450-18-5), or vehicle (ethanol and DMSO) overnight. Cells were then co-
404 incubated with 20 μM YnMyr, 30 μM 17-ODYA, or vehicle and 20 μM MG132 (EMD Millipore 474787-
405 10MG) for 4 hours before washed twice in PBS and frozen at -80 °C. Cells were lysed in 400 μL TEA lysis
406 buffer (50 mM TEA pH 7.4, 150 mM NaCl, 1% triton X-100, and 1 mM PMSF) by inverting for 15 minutes
407 at 4 °C. Lysates were passed five times through a 27-gauge needle, centrifuged at 16,000 x *g* for 15 minutes
408 at 4 °C and protein content determined by Pierce BCA protein assay kit (Thermo Fisher Scientific 23225).
409 25 μg total lysate was removed as input and 0.5 mg total protein was incubated with pre-washed magnetic
410 M2 anti-FLAG (Sigma-Aldrich M8823-5ML) beads at 4 °C for 1.5 hours while inverting. Beads were
411 washed 3X with modified RIPA (50 mM TEA pH 7.4, 150 mM NaCl, 1% Triton X-100, 0.1% SDS, and
412 1% sodium deoxycholate) and resuspended in 40 μL 1x PBS. 10 μL of 5x click reaction mix (1x PBS, 0.5
413 mM biotin azide, 5 mM TCEP, 0.5 mM TBTA, 5 mM $CuSO_4$) was added and reactions incubated for 1 hour
414 at 24 °C, shaking at 550 RPM. Beads were washed 3X in modified RIPA and eluted 2X using 30 μL of 1
415 mg/mL FLAG peptide in modified RIPA buffer. 12 μL of non-reducing 6x SDS sample buffer was added
416 to eluate before heating at 95 °C for 2 minutes and analysis by SDS-PAGE. Note that addition of reducing
417 agents to SDS sample buffer results in loss of 17-ODYA signal. Samples were transferred to nitrocellulose
418 membrane and lipidation was detected using fluorophore-tagged streptavidin, and total CLMB with anti-
419 FLAG. Immunoblots were imaged using a Licor Odyssey CLx and quantified with Image Studio software.
420

421 **Metabolic pulse-chase labeling assay to assess dynamic CLMB S-acylation:**

422 HEK293 Flp-In TReX cells stably expressing $CLMB_{WT}$-FLAG were induced with 10 ng/mL doxycycline
423 for 48 hours. Cells were rinsed 2X in PBS and incubated in methionine free DMEM supplemented with 5%
424 charcoal-stripped FBS, 1 mM L-glutamate, 1 mM sodium pyruvate, 0.4 mM cysteine and 10 ng/mL
425 doxycycline along with vehicle (ethanol), 30 μM 17-ODYA, 50 μM L-AHA, or 17-ODYA and L-AHA
426 together. After two hours, cells were washed 2X in PBS and either harvested immediately or incubated in
427 standard media supplemented with 10 μM palmitic acid and 10 ng/mL doxycycline, with or without 10 μM

428 palmostatin B (EMD Millipore 178501-5MG). Cells were rinsed in PBS and frozen at -80 °C. Metabolic
429 labeling was done as described in the previous section with the exception that two rounds of labeling were
430 done. First, Cy5-azide (Click Chemistry Tools AZ118-1) was linked to 17-ODYA. Then, cells were washed
431 and L-AHA was linked to AF-488 (Click Chemistry Tools 1277-1) alkyne before being washed three
432 additional times and eluted using FLAG peptide. Samples were resolved via SDS-PAGE and in-gel
433 fluorescence was read using the GE Amersham Typhoon imaging system. Images were quantified in Image
434 Studio. The proportion of S-acylated CLMB is calculated as Cy5/A-488 normalized to the no chase control.
435

436 **Acyl-PEG exchange:**

437 HEK293 Flp-In TReX lines stably expressing $CLMB_{WT}$, $CLMB_{C7S}$, $CLMB_{C7,14S}$, or $CLMB_{G2A}$ were induced
438 with 10 ng/mL doxycycline for 48 hours. Cells were rinsed 2X in PBS and stored at -80 °C. Cells were
439 lysed in 400 µL lysis buffer (50 mM TEA pH 7.3, 150 mM NaCl, 2.5% SDS, 1 mM PMSF, 100 units
440 benzonase) at 37 °C for 20 minutes, shaking at 800 RPM. Lysates were passed 10X through a 27-gauge
441 needle, centrifuged at 16,000 x *g* for 5 minutes and protein quantified by BCA. Lysates were adjusted to 2
442 mg/mL and incubated with 10 mM TCEP for 30 minutes at room temperature. Cysteines were protected by
443 incubating with 25 mM NEM for 2 hours at 40 °C, shaking at 800RPM. Protein was precipitated over night
444 with four volumes of acetone at -20 °C, centrifuged at 16,000 x *g* for 20 minutes at 4 °C and washed 4X in
445 70% acetone. Acetone was removed, pellets air-dried to remove all traces of acetone and resuspended in 75
446 µL Buffer A (50 mM TEA pH 7.3, 150 mM NaCl, 4% SDS, 0.2% triton X-100, 4 mM EDTA) for 1 hour at
447 40 °C, shaking at 800 RPM. Samples were centrifuged at 16,000 x *g* for 2 minutes, 7 µL removed as input,
448 and the remainder split into +cleavage and -cleavage fractions. The +cleavage sample containing 1% SDS
449 was treated with 750 µM hydroxylamine (final concentration) for 1 hour at 30 °C, rotating end over end.
450 Following methanol-chloroform precipitation (ice cold, final concentrations 42% methanol, 16%
451 chloroform) samples were centrifuged at 16,000 x *g* for 20 minutes at 4 °C, aqueous layer removed, washed
452 3X with 100% methanol and air dried. Pellets were resuspended as described in Buffer A and incubated in
453 1 mM mPEG-Mal (Methoxypolyethylene glycol maleimide, 5 kDa, 63187 Sigma-Aldrich) for 2 hours at

454 room temp, rotating end over end. Samples were methanol-chloroform precipitated as described,
455 resuspended in Lysis buffer with 1X SDS-PAGE sample buffer, resolved using SDS-PAGE and visualized
456 via immunoblotting with mouse anti-FLAG to detect CLMB-FLAG. Endogenous calnexin was detected
457 using anti-calnexin antibodies. Immunoblots were imaged using a Licor Odyssey CLx and quantified with
458 Image Studio software.
459
460 **Detergent-assisted subcellular fractionation:**
461 HEK293 Flp-In TReX lines stably expressing $CLMB_{WT}$, $CLMB_{C7,14S}$, or $CLMB_{G2A}$ were induced with 10
462 ng/mL doxycycline for 48 hours and 20 µM MG132 (EDM Millipore 474787-10MG) for 4 hours prior to
463 harvesting. Cells were washed 2X in PBS, harvested and immediately lysed in 600 µL of Cytoplasm Buffer
464 (10 mM HEPES pH 6.8, 100 mM NaCl, 300 mM sucrose, 3 mM $MgCl_2$, 5 mM EDTA, 0.015% digitonin,
465 1x halt protease inhibitor cocktail (Thermo Fischer scientific 78442)) at 4 °C for 15 minutes. 60 µL of total
466 lysate was removed as input and the remainder centrifuged at 1000 x *g* for 10 min at 4 °C. The supernatant
467 was removed as cytoplasmic fraction and the pellet washed 2X in PBS and resuspended in 600 µL
468 membrane buffer (10 mM HEPES pH 7.5, 100 mM NaCl, 300 mM sucrose, 3 mM $MgCl_2$, 3 mM EDTA,
469 0.5% Triton X-100, 1x halt protease inhibitor cocktail) for 30 minutes at 4 °C turning end over end.
470 Insoluble material was pelleted by centrifugation at 5000 x *g* for 10 minutes at 4 °C and supernatant
471 removed as membrane fraction. Both fractions were centrifuged at 12,000 x *g* at 4 °C for 10 minutes.
472 Samples were heated in 1X SDS sample buffer at 95 °C for 5 minutes, resolved via SDS-PAGE,
473 immunoblotted and CLMB-FLAG detected using anti-FLAG antibodies; anti-GM130 and anti-α-tubulin
474 were used as membrane and cytosolic markers respectively. Immunoblots were imaged using a Licor
475 Odyssey CLx and quantified with Image Studio software. CLMB in cytosolic and membrane fractions were
476 quantified as $CLMB_{Cyto}/(CLMB_{Cyto}+ CLMB_{Mem})$ and $CLMB_{Mem}/(CLMB_{Cyto} + CLMB_{Mem})$, respectively.
477
478 **Immunofluorescence, microscopy, and image analysis:**

479 MCF7 cells were co-transfected (as described previously) with equal amounts of pcDNA5 encoding
480 $CLMB_{WT}$, $CLMB_{IxITMut}$, $CLMB_{LxVMut}$, $CLMB_{T44A}$ and pcDNA5 encoding CNA-GFP. The following day
481 cells were plated on poly-lysine coated 12 mm, #1.5H glass coverslips (ThorLabs). On day three, cells were
482 washed in PBS and fixed in 100% methanol for 10 minutes at -20 °C. Coverslips were washed 3 times in
483 1x PBS, blocked (1x PBS, 200 mM glycine, 2.5% FBS) for 30 minutes at room temperature, then incubated
484 in primary antibody diluted in blocking buffer for 1 hour before being washed 3 times in 1x PBS and
485 incubated for 1 hour in secondary antibody solution. Following three additional washes, coverslips were
486 mounted using Prolong Glass mountant with NucBlue stain. After sitting overnight at room temperature,
487 coverslips were imaged using a Lionheart FX automated widefield microscope with a 20X Plan Fluorite
488 WD 6.6 NP 0.45 objective. For each coverslip, a 7 by 7 grid of non-overlapping images was automatically
489 taken. All images were manually assessed and those with defects (debris, bubbles, out-of-focus, etc.) were
490 filtered out. Images were analyzed using an automated pipeline using CellProfiler [52]. Briefly, cells were
491 identified by their nuclei and all those lacking CLMB-FLAG staining removed. CLMB-FLAG signal was
492 used to define the cell body and all cells containing one or more fully saturated pixels in the CLMB-FLAG
493 or CNA-GFP channels were removed. Pearson's correlation coefficient between CLMB-FLAG and CNA-
494 GFP was determined for each individual cell. >500 cells per condition were analyzed.
495
496 **GFP-Trap coimmunoprecipitation:**
497 HEK293 cells were co-transfected (as described previously) with pcDNA5 encoding CNA-GFP and
498 pcDNA5 encoding $CLMB_{WT}$, $CLMB_{IxITMut}$, $CLMB_{LxVMut}$, $CLMB_{T44A}$, or $CLMB_{LxVMut+T44A}$. 24 hours post-
499 transfection, cells were washed 2X in PBS and frozen at -80 °C. Cells were lysed in 500 µL lysis buffer (50
500 mM Tris pH 7.5, 150 mM NaCl, 1% NP-40), aspirated 5X with a 27-gauge needle, centrifuged at 16,000 x
501 *g* for 20 min at 4 °C and protein quantified via BCA. 100 mg total protein was removed as input. Lysates
502 were adjusted to 0.5% NP-40 and 500 µg of protein incubated with pre-washed magnetic GFP-TRAP beads
503 (ChromoTek gtma-20) for 2 hours at 4 °C, turning end over end. Beads were magnetized, washed 3 times
504 and eluted with 50 µL of 2x SDS PAGE sample buffer. Samples were resolved via SDS-PAGE and

505 visualized via immunoblotting with anti-flag antibodies to detect CLMB-FLAG and anti-GFP to detect
506 CNA-GFP. Anti-GAPDH was used as a loading control for inputs. Immunoblots were imaged using a Licor
507 Odyssey CLx and CLMB-calcineurin binding was quantified with Image Studio software. Co-purified
508 CLMB was normalized using the following: ($CLMB_{IP}/CLMB_{Input}$)/GFP-CNA_{IP}. Additionally, all values are
509 displayed relative to $CLMB_{WT}$ which is set at 1.
510
511 **Protein expression and purification:**
512 CNA catalytic dead mutant H151Q with an N-terminal His_6-CNA (residues 1–391) and CNB (residues 1–
513 170) subunits were expressed using *E. coli* BL21(DE3) cells in Lysogeny Broth (LB) supplemented with
514 50 µg/mL ampicillin. Protein expression was induced with 1 mM isopropyl β-d-1-thiogalactopyranoside
515 (IPTG) at 18 °C. Cells were lysed using a Fisherbrand™ Model 505 Sonic Dismembrator and lysates were
516 centrifuged at 46,000 × *g* at 4 °C for 45 minutes. The protein was purified by incubation with nickel-
517 nitriloacetic acid (Ni-NTA) agarose resin (Qiagen) for 3h at 4 °C. The resin was washed with 50 mM Tris
518 pH 8.0, 250 mM NaCl, 20 mM imidazole, and 1 mM TCEP. A buffer containing 50 mM Tris pH 8.0, 250
519 mM NaCl, 300 mM imidazole, and 1 mM TCEP was used for elution. Calcineurin was further purified by
520 SEC (Superdex® 200 Increase 10/300 GL) using Phosphate-buffered saline (PBS) and $CaCl_2$ 1mM as the
521 final buffer.
522
523 **Fluorescence polarization binding assay:**
524 All FP measurements were performed on a multifunctional microplate reader (EnVision, Perkin Elmer) in
525 black 384-well microplates (Corning, Cat No 3575) with 30 µL of the assay solution per well. 480-nm
526 excitation and 535-nm emission filters were used for the FP measurements. In the FP saturation binding
527 experiments, 5 nM FITC labeled peptides were mixed with increasing concentrations of calcineurin in PBS
528 buffer (pH 7.4) (commercially available tablets, Thermo Fisher #18912014) and 500 µM $CaCl_2$ buffer (from
529 0 to 25 µM). Where indicated (Supplemental Fig. 3), these analyses were carried out at different pHs using
530 a buffer with 20 mM Hepes pH 6.9, 100 mM NaCl, 0.5 mM EDTA, 1 mM TCEP or a buffer containing 50

531 mM HEPES, pH 8.0, 150 mM NaCl, 1 mM TCEP, 500μM $CaCl_2$. FP values were plotted against the log
532 of the protein concentrations, and the dissociation constant (apparent K_D) was obtained from the resulting
533 sigmoidal curve as analyzed in GraphPad Prism 10. Protein concentrations above 5μM resulted in an upturn
534 in fluorescence polarization signal, indicative of possible aggregation or artifacts; to maintain assay
535 integrity, the considered concentrations were limited to ≤5μM.
536
537 **Fluorescence polarization competition assay:**
538 For the competitive binding assay, a mixture containing 5 nM FITC-labeled CLMB peptides and CNA/B
539 (0.08 and 2 μM for CLMB vs PVIVIT experiments) was incubated with serial dilutions of unlabeled
540 peptides for 30 minutes at room temperature. The FP values were determined, and the IC_{50} values, i.e., the
541 concentrations required for 50% displacement of the FITC-labeled peptide, were calculated in GraphPad
542 Prism 10. The K_i values of competitive inhibitors were calculated based on a previously reported method[53],
543 further adapted by[54]. Briefly, the relation of K_i and IC_{50} in competitive inhibition as applied to protein-
544 ligand–inhibitor (P–L–I) interactions, can be summarized by the following equation:
545

$$K_i = \frac{IC_{50}}{(\frac{\mathrm{L}}{K_d} + 1)}$$

546 Where L stands for the concentration of ligand, i.e., the FITC-labeled peptide used in the FP binding assay;
547 and K_D corresponds to the dissociation constant of the same FITC-labeled peptide resulting from the
548 performed FP binding assay.
549
550 **ITC measurements:**
551 Isothermal titration calorimetry (ITC) experiments were performed using an Affinity ITC from TA
552 Instruments (New Castle, DE) equipped with an autosampler in a buffer containing 50 mM HEPES, pH
553 8.0, 150 mM NaCl, 1 mM TCEP, 500μM $CaCl_2$ at 25 °C. 40 μM protein solution in the calorimetric cell
554 was titrated with 100 μM peptide solution using 0.5 μL injection in 200-sec intervals using stirring speed
555 at 125rpm. The resulting isotherm was fitted with a single site model to yield thermodynamic parameters

556 of ΔH, ΔS, stoichiometry, and K_D using NanoAnalyze software (TA instruments). All results are
557 representative of three independent experiments (n = 3).
558
559 **NMR analyses:**
560 All NMR data were acquired using TopSpin3.4 (Bruker), processed with NMRPipe v.2020/2021 and
561 analyzed with CCPNmr v3[55, 56]. Structural biology applications were compiled by the SBGrid consortium.
562 Three-dimensional (3D) NMR experiments were conducted on a Bruker spectrometer operating at 600
563 MHz, equipped with TCI cryoprobes and z-shielded gradients. Samples of approximately180-μM 2H-, ^{13}C-
564 and ^{15}N-calcimembrin in 20 mM Hepes pH 6.9, 100 mM NaCl, 0.5 mM EDTA, 1 mM TCEP and 5% v/v
565 ^{2}H2O were used. Temperature was set to 25˚C. Chemical shift assignments are deposited in the Biological
566 Magnetic Resonance Bank (BMRB) under accession code 52641.

567 The NMR titration samples were prepared by adding unlabeled calcineurin A/B complex or unlabeled
568 calcineurin subunit A into solutions of U-[^{15}N]-labeled calcimembrin (50 μM) to reach a ratio of 0.5:1 (25
569 μM unlabeled calcineurin) or 1:1 (50 μM unlabeled calcineurin). Titration experiments featuring
570 $pCLMB_{LxVMut}$ (40μM) peptide with free CLMB (50μM), and with calcineurin:CLMB at 1:1 and 0.5:1
571 stoichiometries were also performed. Two-dimensional (2D) spectra were acquired using SOFAST-HMQC
572 on a Bruker 800 MHz Avance III spectrometer equipped with a TXO cryoprobe and z-shielded gradients[57].
573 Data was processed using NmrPipe and analyzed with CCPNmr. Secondary structure prediction was
574 analyzed using TALOS-N[58] and CheSPI[24].
575
576 **AlphaFold 3 modeling:**
577 Calcineurin-CLMB complex modeling was done using AlphaFold 3 on AlphaFold server[27]. Modeling was
578 done using truncated CNA_{1-391}, CNB, and two copies of CLMB, either unmodified or phosphorylated at
579 Thr44. Zn^{2+} and Fe^{3+} (found in the calcineurin active site) and four Ca^{2+} ions (bound to CNB) were included
580 in modeling. All images were generated in UCSF ChimeraX 1.8[59].

581

582 ***In vivo* analysis of CLMB phosphorylation status:**

583 HEK293 FLIP-In TreX cells stably expressing $CLMB_{WT}$-FLAG, $CLMB_{IxITMut}$-FLAG, $CLMB_{LxVMut}$-FLAG,
584 or $CLMB_{T44A}$-FLAG were transfected with empty vector or pcDNA5 FRT TO encoding CNA-GFP
585 alongside empty vector or pcDNA5 FRT TO encoding $CLMB_{WT}$-V5, $CLMB_{IxITMut}$-V5, or $CLMB_{LxVMut}$-V5.
586 Protein expression was induced for 24 hours with 10 ng/mL doxycycline, cells washed 2X in PBS and
587 stored at -80 °C. Cells were lysed (50 mM Tris pH 8, 150 mM NaCl, 1% NP-40, 0.1% SDS, 0.5% sodium
588 dodecyl sulfate, 1x Halt protease inhibitor cocktail) and resolved via SDS-PAGE and detected via
589 immunoblotting.

590

591 ***In vitro* CLMB phosphopeptide dephosphorylation:**

592 $CLMB_{WT}$, $CLMB_{IxITMut}$, and $CLMB_{LxVMut}$ phospho-peptides were synthesized by Vivitide, resuspended in
593 10 mM Tris pH 8.0 and dephosphorylated at 26 °C in reaction buffer (50 mM Tris pH 8.0, 100 mM NaCl,
594 6 mM $MgCl_2$, 2 mM $CaCl_2$, 1 mM EGTA, 0.1 mg/mL BSA, 1 mM DTT, 0.5 µM MDCC-PBP (Thermo
595 Scientific PV4406), 1 µM CaM (Millipore Sigma 208694-1MG)). Reactions were initiated by addition of
596 CLMB peptide to a final concentration of 100nM. Reactions took place in a total of 50 µL in a corning
597 black 96 well vessel and were monitored continuously via fluorescence emitted by phosphate bound
598 MDCC-PBP (EX:425/ EM:460). Phosphate standards were used to convert fluorescence intensity to
599 phosphate concentration. Data were analyzed using Prism software. Because the experimental design does
600 not comply with assumptions of standard kinetic models, reaction rates were obtained by fitting data to a
601 single exponential model as an empirical description of the curves to facilitate comparison between
602 experimental conditions.

603

604 ***In vitro* RII phospho-peptide dephosphorylation:**

605 1 µM RII peptide was dephosphorylated at 26 °C in reaction buffer (50 mM Tris pH 8.0, 100 mM NaCl, 6
606 mM $MgCl_2$, 2 mM $CaCl_2$, 1 mM EGTA, 0.1 mg/mL BSA, 1 mM DTT, 0.5 µM MDCC-PBP (Thermo

607 Scientific PV4406), 100nM calmodulin, 10 nM calcineurin, and CLMB peptide at the indicated
608 concentrations (Millipore Sigma 208694-1MG)). Reactions were initiated by adding Ca^{2+} and CaM to their
609 final concentrations. Reactions took place in a total of 50 µL in a corning black 96 well vessel and were
610 monitored continuously via fluorescence emitted by phosphate bound MDCC-PBP (EX:400/ EM:460).
611 Phosphate standards were used to convert fluorescence intensity to phosphate concentration.
612
613 **Kinetic Modeling:**
614 Dephosphorylation data were fit by simulation and non-linear regression using Kintek Explorer™. Sigma
615 values for each individual replicate were obtained using the double exponential afit function. All replicates
616 were simultaneously fit to the models described in Supplemental Fig.s 8 (a,b). Curve offsets were capped
617 at a maximum offset of 50nM. Substrate concentration was allowed to vary by 15% during fitting. Initial
618 parameter values were chosen based on previously published rates, when available. The final offset and
619 initial substrate concentration values for each curve, along with fitting information, are shown in
620 Supplemental Tables 1-3. Final graphs display averaged ($n \geq 5$) phosphate released at each timepoint with
621 the corresponding fit. Simulated data were exported using 200 simulation steps and plotted using GraphPad
622 Prism.
623
624 **Statistical analysis**
625 Statistical analysis was done using Graphpad Prism version 10.2.2. All data is displayed as representative
626 images or mean values with standard deviation error bars unless otherwise noted. All data represent three
627 independent experiments unless otherwise indicated in figure legends. Image analysis of CLMB-calcineurin
628 colocalization (Fig. 2C) was conducted using the following number of cells: $CLMB_{WT}$ = 525, $CLMB_{IxITMut}$
629 = 641, $CLMB_{LxVMut}$ = 500, $CLMB_{T44A}$ = 517. Statistical significance was calculated using one-way analysis
630 of variance (ANOVA) with corrections for multiple comparisons as indicated.
631
632 **Data availability:**

633 All original scans of immunoblots, immunofluorescence images, and AlphaFold predictions can be
634 accessed through Mendeley Data (to be made available upon publication). Plasmids and reagents will be
635 shared upon request. NMR chemical shift assignments are deposited in the Biological Magnetic Resonance
636 Bank (BMRB) under accession code 52641.

637

638 **Acknowledgements:**

639 We thank Norman Davey and members of the Cyert and Arthanari labs, in particular Angela Barth and
640 Sneha Roy, for helpful discussion. We are especially grateful to Rick Russell (UT Austin) for feedback on
641 the kinetic modeling and thank Callie Wigington and Makena Pule for their early contributions to the
642 project. We thank Ilya Bezprozvanny (UT Southwestern) for suggesting the name, calcimembrin.

643

644 **Funding:**

645 MSC, DAB and RYM are supported by NIH grant R35 GM136243. DAB also acknowledges support from
646 NIH grant T32 GM007276. HA, JCR, SQ and TV acknowledge grant R01 GM136859 from NIH.

647

648 **Author Contributions:**

649 MSC, DAB, HA and JCR conceived the studies. SQ and TV provided early NMR analysis of CLMB-
650 calcineurin complexes. DAB, supervised by MSC, carried out experiments and analyzed data for Figures
651 1, 2, and 5, and prepared figures. RYM, supervised by MSC, carried out experiments and analyzed data for
652 Supplementary figures 1 and 2a. JCR, supervised by HA, carried out experiments and analyzed data for
653 Figures 3 and 4. TV carried out secondary structure analyses. DAB and MSC wrote the manuscript in
654 consultation with HA and JCR.

655

656 **References**

657 1. Bootman MD, Bultynck G. Fundamentals of Cellular Calcium Signaling: A Primer. *Cold*
658 *Spring Harb Perspect Biol* **12**, (2020).

659
660 2. Ulengin-Talkish I, Cyert MS. A cellular atlas of calcineurin signaling. *Biochim Biophys*
661 *Acta Mol Cell Res* **1870**, 119366 (2023).

662
663 3. Aramburu J, Rao A, Klee CB. Calcineurin: from structure to function. *Curr Top Cell*
664 *Regul* **36**, 237-295 (2000).

665
666 4. Grigoriu S*, et al.* The molecular mechanism of substrate engagement and
667 immunosuppressant inhibition of calcineurin. *PLoS Biol* **11**, e1001492 (2013).

668
669 5. Roy J, Cyert MS. Identifying New Substrates and Functions for an Old Enzyme:
670 Calcineurin. *Cold Spring Harb Perspect Biol* **12**, (2020).

671
672 6. Brauer BL*, et al.* Leveraging New Definitions of the LxVP SLiM To Discover Novel
673 Calcineurin Regulators and Substrates. *ACS Chem Biol* **14**, 2672-2682 (2019).

674
675 7. Sheftic SR, Page R, Peti W. Investigating the human Calcineurin Interaction Network
676 using the piLxVP SLiM. *Sci Rep* **6**, 38920 (2016).

677
678 8. Tsekitsidou E*, et al.* Calcineurin associates with centrosomes and regulates cilia length
679 maintenance. *J Cell Sci* **136**, (2023).

680
681 9. Wigington CP*, et al.* Systematic Discovery of Short Linear Motifs Decodes Calcineurin
682 Phosphatase Signaling. *Mol Cell* **79**, 342-358 e312 (2020).

683
684 10. Nakamura T*, et al.* Overexpression of C16orf74 is involved in aggressive pancreatic
685 cancers. *Oncotarget* **8**, 50460-50475 (2017).

686
687 11. Meinnel T, Dian C, Giglione C. Myristoylation, an Ancient Protein Modification
688 Mirroring Eukaryogenesis and Evolution. *Trends Biochem Sci* **45**, 619-632 (2020).

689
690 12. Blanc M, David FPA, van der Goot FG. SwissPalm 2: Protein S-Palmitoylation Database.
691 *Methods Mol Biol* **2009**, 203-214 (2019).

692
693 13. Yap MC*, et al.* Rapid and selective detection of fatty acylated proteins using omega-
694 alkynyl-fatty acids and click chemistry. *J Lipid Res* **51**, 1566-1580 (2010).

695
696 14. Wang Y, Windh RT, Chen CA, Manning DR. N-Myristoylation and betagamma play roles
697 beyond anchorage in the palmitoylation of the G protein alpha(o) subunit. *J Biol Chem*
698 **274**, 37435-37442 (1999).

15. Dekker FJ, *et al.* Small-molecule inhibition of APT1 affects Ras localization and signaling. *Nat Chem Biol* **6**, 449-456 (2010).

16. Percher A, Ramakrishnan S, Thinon E, Yuan X, Yount JS, Hang HC. Mass-tag labeling reveals site-specific and endogenous levels of protein S-fatty acylation. *Proc Natl Acad Sci U S A* **113**, 4302-4307 (2016).

17. F.S. M, Abrami L, Linder ME, Bamji SX, Dickinson BC, van der Goot FG. Mechanisms and functions of protein S-acylation. *Nat Rev Mol Cell Biol*, (2024).

18. Hornbeck PV, *et al.* 15 years of PhosphoSitePlus(R): integrating post-translationally modified sites, disease variants and isoforms. *Nucleic Acids Res* **47**, D433-D441 (2019).

19. Blumenthal DK, Takio K, Hansen RS, Krebs EG. Dephosphorylation of cAMP-dependent protein kinase regulatory subunit (type II) by calmodulin-dependent protein phosphatase. Determinants of substrate specificity. *J Biol Chem* **261**, 8140-8145 (1986).

20. Perrino BA, Ng LY, Soderling TR. Calcium regulation of calcineurin phosphatase activity by its B subunit and calmodulin. Role of the autoinhibitory domain. *J Biol Chem* **270**, 7012 (1995).

21. Aramburu J, Yaffe MB, Lopez-Rodriguez C, Cantley LC, Hogan PG, Rao A. Affinity-driven peptide selection of an NFAT inhibitor more selective than cyclosporin A. *Science* **285**, 2129-2133 (1999).

22. Li H, Zhang L, Rao A, Harrison SC, Hogan PG. Structure of calcineurin in complex with PVIVIT peptide: portrait of a low-affinity signalling interaction. *J Mol Biol* **369**, 1296-1306 (2007).

23. Shen Y, Bax A. Protein backbone and sidechain torsion angles predicted from NMR chemical shifts using artificial neural networks. *J Biomol NMR* **56**, 227-241 (2013).

24. Nielsen JT, Mulder FAA. CheSPI: chemical shift secondary structure population inference. *J Biomol NMR* **75**, 273-291 (2021).

25. Solyom Z, Schwarten M, Geist L, Konrat R, Willbold D, Brutscher B. BEST-TROSY experiments for time-efficient sequential resonance assignment of large disordered proteins. *J Biomol NMR* **55**, 311-321 (2013).

739 26. Hendus-Altenburger R*, et al.* Molecular basis for the binding and selective
740 dephosphorylation of Na(+)/H(+) exchanger 1 by calcineurin. *Nat Commun* **10**, 3489
741 (2019).

742
743 27. Abramson J*, et al.* Accurate structure prediction of biomolecular interactions with
744 AlphaFold 3. *Nature* **630**, 493-500 (2024).

745
746 28. Shibasaki F, Price ER, Milan D, McKeon F. Role of kinases and the phosphatase
747 calcineurin in the nuclear shuttling of transcription factor NF-AT4. *Nature* **382**, 370-373
748 (1996).

749
750 29. Li H, Rao A, Hogan PG. Structural delineation of the calcineurin-NFAT interaction and
751 its parallels to PP1 targeting interactions. *J Mol Biol* **342**, 1659-1674 (2004).

752
753 30. Johnson KA. Fitting enzyme kinetic data with KinTek Global Kinetic Explorer. *Methods*
754 *Enzymol* **467**, 601-626 (2009).

755
756 31. Klee CB, Draetta GF, Hubbard MJ. Calcineurin. *Adv Enzym* **61**, 149-200 (1988).

757
758 32. Jespersen N, Barbar E. Emerging Features of Linear Motif-Binding Hub Proteins. *Trends*
759 *Biochem Sci* **45**, 375-384 (2020).

760
761 33. Li H, Rao A, Hogan PG. Interaction of calcineurin with substrates and targeting proteins.
762 *Trends Cell Biol* **21**, 91-103 (2011).

763
764 34. Lee S*, et al.* The optimized core peptide derived from CABIN1 efficiently inhibits
765 calcineurin-mediated T-cell activation. *Exp Mol Med* **54**, 613-625 (2022).

766
767 35. Nguyen HQ*, et al.* Quantitative mapping of protein-peptide affinity landscapes using
768 spectrally encoded beads. *Elife* **8**, (2019).

769
770 36. O'Brien KT, Mooney C, Lopez C, Pollastri G, Shields DC. Prediction of polyproline II
771 secondary structure propensity in proteins. *R Soc Open Sci* **7**, 191239 (2020).

772
773 37. Tubiana J*, et al.* Funneling modulatory peptide design with generative models: Discovery
774 and characterization of disruptors of calcineurin protein-protein interactions. *PLoS*
775 *Comput Biol* **19**, e1010874 (2023).

776

38. Aramburu J, Garcia-Cozar F, Raghavan A, Okamura H, Rao A, Hogan PG. Selective inhibition of NFAT activation by a peptide spanning the calcineurin targeting site of NFAT. *Mol Cell* **1**, 627-637 (1998).

39. Li SJ*, et al.* Cooperative autoinhibition and multi-level activation mechanisms of calcineurin. *Cell Res* **26**, 336-349 (2016).

40. Oliveria SF, Dell'Acqua ML, Sather WA. AKAP79/150 anchoring of calcineurin controls neuronal L-type Ca2+ channel activity and nuclear signaling. *Neuron* **55**, 261- 275 (2007).

41. Li H, Pink MD, Murphy JG, Stein A, Dell'Acqua ML, Hogan PG. Balanced interactions of calcineurin with AKAP79 regulate Ca2+-calcineurin-NFAT signaling. *Nat Struct Mol Biol* **19**, 337-345 (2012).

42. Church TW*, et al.* AKAP79 enables calcineurin to directly suppress protein kinase A activity. *Elife* **10**, (2021).

43. Huang WYC, Boxer SG, Ferrell JE, Jr. Membrane localization accelerates association under conditions relevant to cellular signaling. *Proc Natl Acad Sci U S A* **121**, e2319491121 (2024).

44. Johnson JL*, et al.* An atlas of substrate specificities for the human serine/threonine kinome. *Nature* **613**, 759-766 (2023).

45. Li M, Jiang J, Yue L. Functional characterization of homo- and heteromeric channel kinases TRPM6 and TRPM7. *J Gen Physiol* **127**, 525-537 (2006).

46. Goldman A*, et al.* The Calcineurin Signaling Network Evolves via Conserved Kinase-Phosphatase Modules that Transcend Substrate Identity. *Mol Cell* **55**, 422-435 (2014).

47. Hirschi A, Cecchini M, Steinhardt RC, Schamber MR, Dick FA, Rubin SM. An overlapping kinase and phosphatase docking site regulates activity of the retinoblastoma protein. *Nat Struct Mol Biol* **17**, 1051-1057 (2010).

48. Jara KA*, et al.* Multivalency, autoinhibition, and protein disorder in the regulation of interactions of dynein intermediate chain with dynactin and the nuclear distribution protein. *Elife* **11**, (2022).

49. Simonsen S, *et al.* Extreme multivalency and a composite short linear motif facilitate PCNA-binding, localisation and abundance of p21 (CDKN1A). *FEBS J*, (2025).

50. Dinh J, *et al.* The microprotein C16orf74/MICT1 promotes thermogenesis in brown adipose tissue. *EMBO J*, (2025).

51. Uhlen M, *et al.* Towards a knowledge-based Human Protein Atlas. *Nat Biotechnol* **28**, 1248-1250 (2010).

52. Stirling DR, Swain-Bowden MJ, Lucas AM, Carpenter AE, Cimini BA, Goodman A. CellProfiler 4: improvements in speed, utility and usability. *BMC Bioinformatics* **22**, 433 (2021).

53. Cheng Y, Prusoff WH. Relationship between the inhibition constant (K1) and the concentration of inhibitor which causes 50 per cent inhibition (I50) of an enzymatic reaction. *Biochem Pharmacol* **22**, 3099-3108 (1973).

54. Cer RZ, Mudunuri U, Stephens R, Lebeda FJ. IC50-to-Ki: a web-based tool for converting IC50 to Ki values for inhibitors of enzyme activity and ligand binding. *Nucleic Acids Res* **37**, W441-445 (2009).

55. Delaglio F, Grzesiek S, Vuister GW, Zhu G, Pfeifer J, Bax A. NMRPipe: a multidimensional spectral processing system based on UNIX pipes. *J Biomol NMR* **6**, 277-293 (1995).

56. Vranken WF, *et al.* The CCPN data model for NMR spectroscopy: development of a software pipeline. *Proteins* **59**, 687-696 (2005).

57. Schanda P, Kupce E, Brutscher B. SOFAST-HMQC experiments for recording two-dimensional heteronuclear correlation spectra of proteins within a few seconds. *J Biomol NMR* **33**, 199-211 (2005).

58. Shen Y, Bax A. Protein structural information derived from NMR chemical shift with the neural network program TALOS-N. *Methods Mol Biol* **1260**, 17-32 (2015).

59. Meng EC, *et al.* UCSF ChimeraX: Tools for structure building and analysis. *Protein Sci* **32**, e4792 (2023).

Figure Legends

855 **Fig. 1 Calcimembrin localizes to membranes via protein lipidation**. **a.** CLMB schematic showing N-
856 myristoylation (red); S-acylation (yellow), phosphorylation (green), calcineurin-binding motifs LxVP
857 (pink) and PxIxIT (purple). Sequences of wild-type and mutated regions shown. **b.** Representative
858 immunoblot showing metabolic labeling of CLMB-Flag (wild-type or indicated mutants) with palmitate
859 (17-ODYA) or myristate (YnMyr) analogs, analyzed via CLICK chemistry with biotin-azide and
860 detection with IRdye 800CW streptavidin ("Biotin"). Inputs and immunoprecipitated (IP) samples are
861 shown. Asterisks indicate CLMB dimers. (n = 3 independent experiments). **c.** Representative immunoblot
862 showing S-acylation of CLMB-FLAG (wild-type or indicated mutants) and endogenous calnexin
863 (positive control) detected via Acyl-PEG exchange. Asterisks show PEGylation events. Input, cleaved
864 (NH_2OH) and PEGylated (mPEG), and non-cleaved PEGylated conditions are indicated (n = 3
865 independent experiments). **d.** Representative in-gel fluorescence scan showing pulse-chase analysis of
866 CLMB-FLAG using palmitate (17-ODYA) or methionine (L-AHA) analogs detected via CLICK
867 chemistry with Cy5 or AZDye 488, respectively. Incorporation into CLMB-FLAG with no analog (Neg
868 Ctrl), at 0 or 30 minutes after unlabeled chase with DMSO (control) or PalmB. shown (n = 3 independent
869 experiments). **e.** Data from (**d**) showing mean ± SEM of 17-ODYA signal normalized to L-AHA; * $p <$
870 0.05, T0 vs PalmB $p = 0.0103$, ** $p < 0.01$, DMSO vs PalmB $p = 0.007$**. f**. Representative immunoblot
871 showing sub-cellular fractionation of CLMB-FLAG (wild-type or indicated mutants) with input,
872 cytoplasmic (cyto), and membrane (mem) fractions. GM130 and α-tubulin mark mem and cyto fractions,
873 respectively (n= 3 independent experiments). **g**. Data from (**f**) showing mean ± SEM cyto or mem signals
874 normalized to total (cyto + mem); n.s. not significant, **** $p < .0001$. $CLMBC_{7,14S}$ vs $CLMB_{G2A}$:
875 cytoplasm, $p = 0.238$, membrane $p = 0.238$. For (**e, g**) p-values were calculated by two-way ANOVA
876 corrected by Tukey's multiple comparison.

877

878 **Fig. 2 Composite LxVPxIxIT SLiM in calcimembrin mediates binding to and dephosphorylation by**

879 **calcineurin. a.** Representative immunoblot showing co-purification of CLMB-FLAG (wild-type and
880 indicated mutants) with CNA-GFP. Inputs and purified (IP) samples shown (n = 3 independent
881 experiments). Glyceraldehyde-3-Phosphate Dehydrogenase (GAPDH) was used as a loading control. **b.**
882 Data from (**a**) showing mean ± SEM of co-purified CLMB-FLAG normalized to CLMB-FLAG input
883 levels and precipitated CNA-GFP. Indicated p-values calculated by two-way ANOVA corrected by
884 Dunnett's multiple comparison test. **** $p < 0.0001$, *** $p<0.001$, * $p<0.05$; $CLMB_{WT}$ vs $CLMB_{LxVmut}$ p
885 = 0.0325, $CLMB_{WT}$ vs $CLMB_{T44A}$ p = 0.0002. **c.** Representative images of MCF7 cells co-transfected
886 with CLMB-FLAG (wild-type or indicated mutants) and CNA-GFP. Fixed cells immunostained with
887 anti-FLAG (magenta), anti-GFP (yellow), and nuclei (DNA) with Hoechst 33342. Scale bar = 50 μm.
888 Arrows indicate some examples of CLMB and CNA co-localization to plasma membrane. Data from (**c**)
889 showing median with 95% CI Pearson's correlation coefficient of CLMB-calcineurin colocalization. Each
890 point represents a single cell ($n \geq 500$ for each condition). p-values calculated by Kruskal-Wallis with
891 Dunn's multiple comparisons correction. * $p < 0.05$ ($p = 0.0116$), ** $p < 0.01$ ($p = 0.0092$), **** $p <$
892 0.0001. **e** Dephosphorylation of $pCLMB_{WT}$ (blue) or $pCLMB_{LxVMut}$ (pink) phosphopeptides with 20 nM
893 CNA/B and 1 μM CaM. Mean ± SEM of phosphate released displayed for ≥ 4 replicates at each timepoint
894 with reaction rate as shown.

895

896 **Fig. 3 Thr44 Phosphorylation and the LxVP motif contribute to PxIxIT binding. a.** Determination
897 of the affinity between CNA/B and unlabeled $pCLMB_{WT}$ peptide using isothermal calorimetry.
898 Dissociation constant (K_D) = 37 ± 1.22 nM, reaction stoichiometry (n value) = 1.00 ± 0.02,
899 enthalpy (ΔH) = -3.97 ± 0.76, and entropy ($T\Delta S$) = 20.8 ± 3.01 are shown. Data are mean ± s.d.
900 for n = 3 independent experiments. **b**. Binding isotherm obtained by titration of unlabeled
901 $pCLMB_{WT}$ peptide into CNA/B (40 μM). **c**. Fluorescence polarization (FP) saturation binding
902 curves of FITC-$pCLMB_{WT}$ and FITC-$CLMB_{WT}$ (5nM) incubated with serial dilutions of CNA/B

903 (0 to 5μM). FP data were fitted to a one-site binding model (mean ± s.d., n = 2 independent
904 experiments). **d**. Competitive binding assay of unlabeled $pCLMB_{WT}$, $CLMB_{WT}$, $pCLMB_{IxITMut}$,
905 and $pCLMB_{LxVMut}$ peptides titrated against FITC-PVIVIT peptide (5 nM) in the presence of 2
906 μM CNA/B. Data are mean ± s.d. of n = 2 independent experiment. **e.** Competitive binding assay
907 of unlabeled $pCLMB_{WT}$, $CLMB_{WT}$, $pCLMB_{IxITMut}$, and $pCLMB_{LxVMut}$ peptides titrated against
908 FITC-$pCLMB_{WT}$ peptide, (5 nM) in the presence of 0.08 μM CNA/B. Data are mean ± s.d. for n
909 = 2 independent experiments**. f.** Table displaying the experimentally obtained IC_{50} values and
910 converted K_i values from data in (**d, e**).

911

912 **Fig. 4 CLMB-calcineurin binding extends beyond the LxVP and PxIxIT motifs. a.** ^{15}N HSQC spectra
913 of free CLMB with the resonance assignment. **b.** NMR spectral analysis of CLMB interaction with CNA
914 at 2:1 (CLMB: CNA); **c**. with CNA at 1:1(CLMB: CNA); **d.** with CNA/B at 2:1 (CLMB: CNA/B); **e**.
915 with CNA/B at 1:1 (CLMB: CNA/B). **b-e.** Graphs display the intensity ratios of CLMB resonances with
916 and without the titrant (CNA or CNA/B) at different molar ratios. The ratios corresponding to the LxV
917 motif (pink) and IxIT (purple) are highlighted. Residues with no access to the intensity ratio are
918 represented with negative numbers, and peaks resulting in complete broadening are shown in green (I/I0
919 = -0.4). Unassigned residues in apo CLMB are blue (I/I0 = -0.2), prolines (which are not represented in
920 ^{15}N-HSQC are grey (I/I0 = -0.2), and residues for which the bound resonance cannot be unambiguously
921 assigned are red, (I/I0 = -0.2). * Residues with I/I0 higher than 1 due to overlapping resonances.

922

923 **Fig. 5 Calcineurin dephosphorylates calcimembrin by forming multimers. a.** Representative
924 immunoblot showing phosphorylation-induced mobility shifts in CLMB-FLAG (wild-type or indicated
925 mutants) when co-expressed with GFP-CNA and CLMB-V5 (wild-type or indicated mutants). GAPDH
926 was used as a loading control **b.** Data from (**a**) showing mean ± SEM phospho-CLMB-FLAG normalized

927 to total CLMB-FLAG. p-values calculated by two-way ANOVA corrected by Dunnett's multiple
928 comparison test (n = 3 independent experiments). n.s., not significant; without vs with $CLMB_{IxIxITmut}$-V5
929 expression: p = 0.995, 0.748, 0.999 from left to right. $CLMB_{IxITmut}$ without vs with CNA-GFP p = 0.626.
930 **** $p < 0.0001$, *** $p < 0.001$, p = 0.0005. **c.** Cartoon representation of calcineurin (turquoise)-CLMB
931 complex formation and CLMB dephosphorylation (removal of pink "P") under conditions in (**a**), i.e.
932 CLMB-FLAG (blue with "F") overexpression with or without co-expression of Calcineurin-GFP and
933 CLMB-V5 (green with "V") as indicated. Top row shows $CLMB_{WT}$-FLAG, bottom row shows
934 $CLMB_{IXITMut}$-FLAG (labelled LDVPxxxx). **d**. (Top) Experimental data showing phosphate released from
935 100 nM $pCLMB_{WT}$ (blue) or $pCLMB_{IxITMut}$ (purple) phosphopeptide dephosphorylated by 20 nM (left),
936 100 nM (middle) or 200 nM (right) CNA/B and 1 μM calmodulin. Each dephosphorylation rate is
937 displayed and data is mean ± SEM for ≥ 5 replicates at each timepoint. (Bottom) Overlay of experimental
938 data (circles) with results of kinetic simulations (solid lines) using the model shown in Fig. S5a, b for
939 each calcineurin concentration.

940

941 **Fig. 6 Models explaining how calcimembrin may modulate calcineurin signaling. a** (1) CLMB
942 localizes to membranes via dynamic acylation where it (2) recruits calcineurin (turquoise). At low CLMB
943 levels, calcineurin remains tightly bound to phosphorylated CLMB (purple) regardless of Ca^{2+} signals. (3)
944 At higher CLMB levels, CLMB (purple and green) forms multimers with calcineurin and is
945 dephosphorylated upon calcineurin activation by Ca^{2+} and CaM. (4) Calcineurin is then released and can
946 engage and dephosphorylate membrane-associated substrates (red) that contain PxIxT and LxVP SLiMs.
947 **b** (1) CLMB localizes to membranes via dynamic acylation where it (2) recruits calcineurin (turquoise).
948 At low CLMB levels, calcineurin remains tightly bound to phosphorylated CLMB (purple). (3) Ca^{2+} and
949 CaM activate calcineurin, allowing it to engage and dephosphorylate LxVP-containing substrates (red).
950 (4) At high CLMB levels (purple and green) calcineurin-CLMB multimers form. (5) This promotes
951 CLMB dephosphorylation and triggers calcineurin release to terminate signaling.

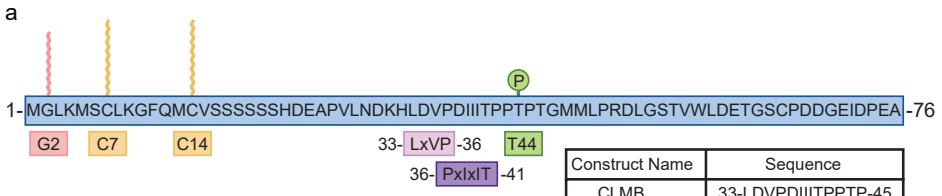

Construct Name	Sequence
$CLMB_{WT}$	33-LDVPDIIITPPTP-45
$CLMB_{LxVMut}$	33-ADAPDIIITPPTP-45
$CLMB_{IxITMut}$	33-LDVPDAIAAPPTP-45

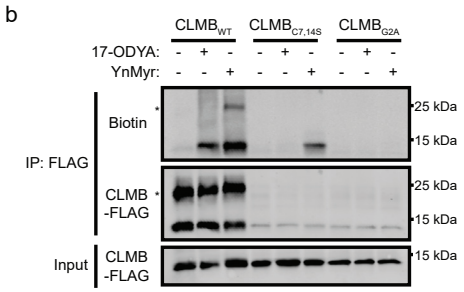

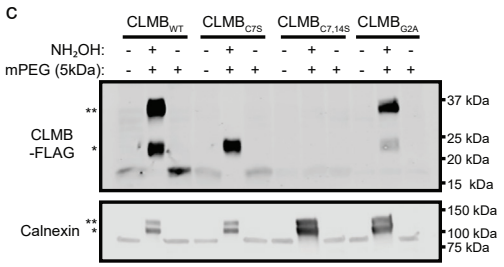

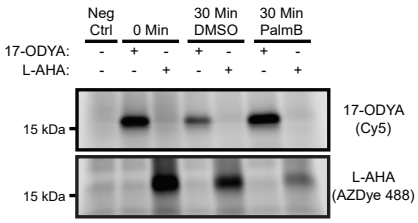

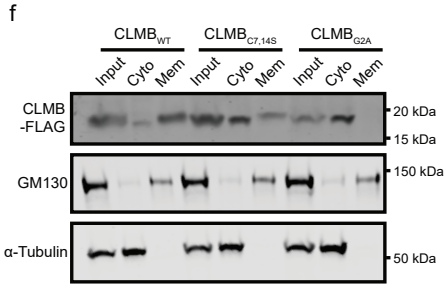

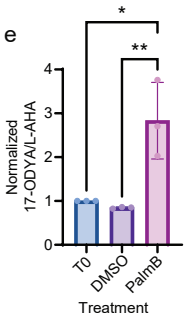

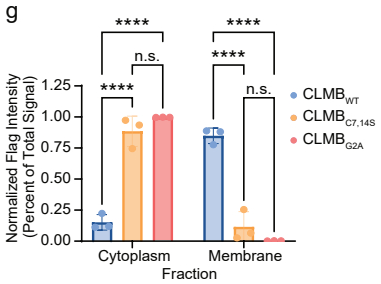

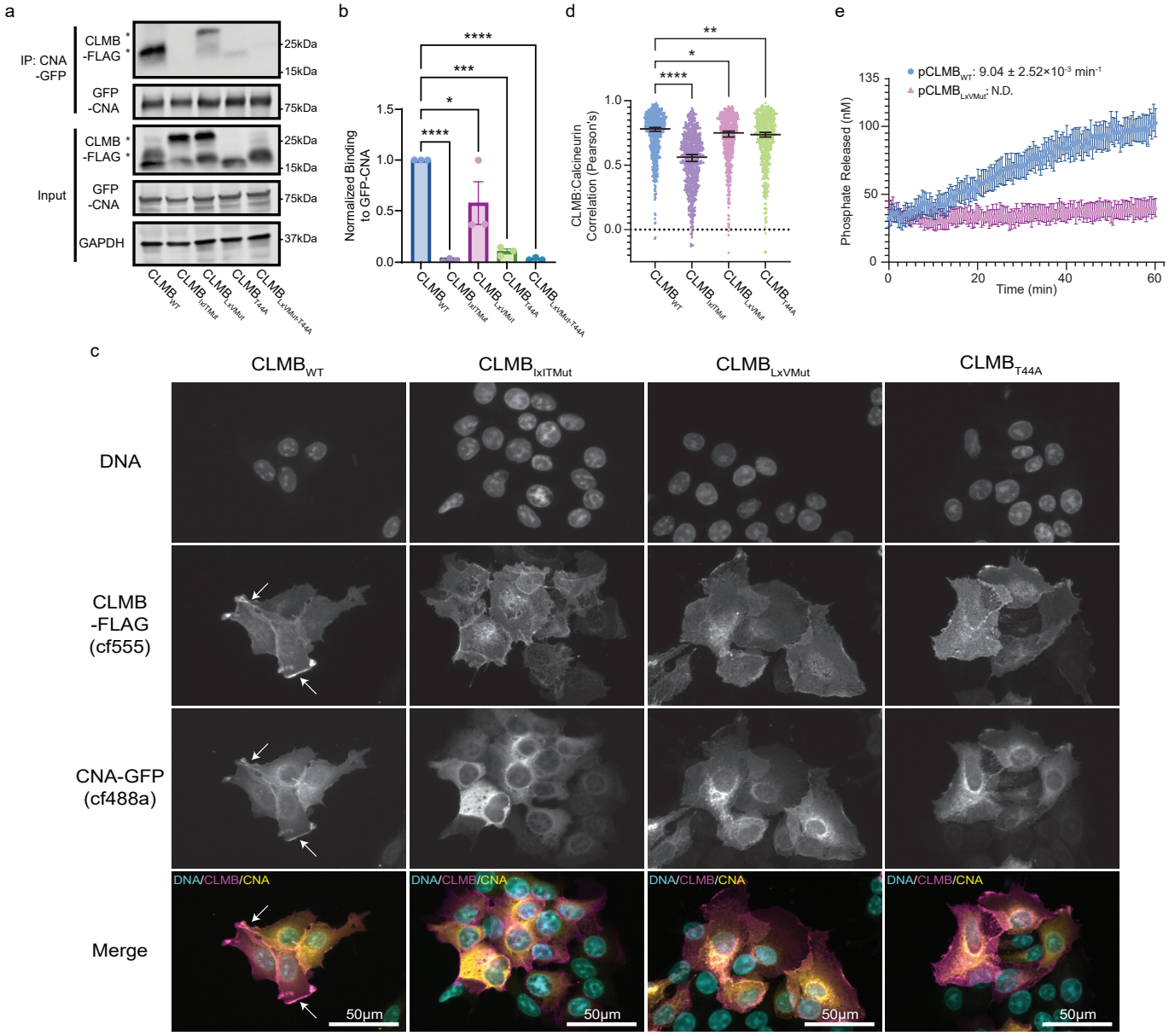
a
IP: CNA -GFP
CLMB -FLAG
GFP -CNA
Input
CLMB -FLAG
GFP -CNA
GAPDH
25kDa
15kDa
75kDa
25kDa
15kDa
75kDa
37kDa
CLMB WT
CLMB IxITMut
CLMB LxVMut
CLMB T44A
CLMB LxVMut-T44A
b
Normalized Binding to GFP-CNA
****
***
*
****
d
CLMB:Calcineurin Correlation (Pearson's)
**
*
****
e
pCLMB WT: 9.04 ± 2.52×10-3 min-1
pCLMB LxVMut: N.D.
Phosphate Released (nM)
Time (min)
c
CLMB WT
CLMB IxITMut
CLMB LxVMut
CLMB T44A
DNA
CLMB -FLAG (cf555)
CNA-GFP (cf488a)
Merge
DNA/CLMB/CNA
50μm

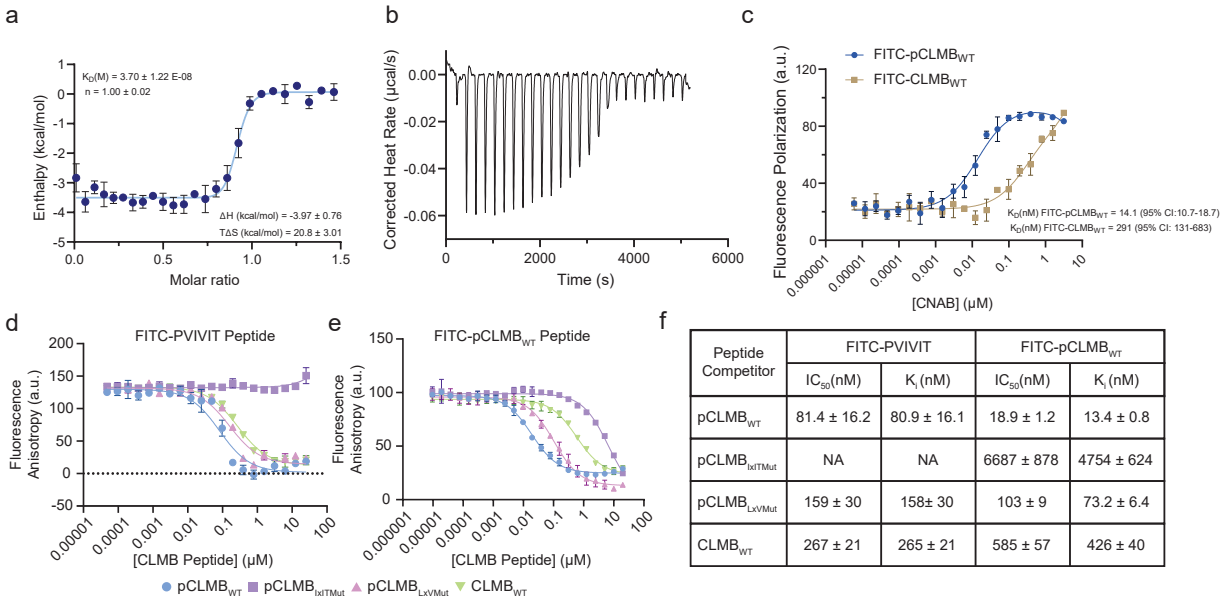

f

Peptide Competitor	FITC-PVIVIT		FITC-pCLMB$_{WT}$	
	IC_{50}(nM)	K_i (nM)	IC_{50}(nM)	K_i (nM)
pCLMB$_{WT}$	81.4 ± 16.2	80.9 ± 16.1	18.9 ± 1.2	13.4 ± 0.8
pCLMB$_{IxITMut}$	NA	NA	6687 ± 878	4754 ± 624
pCLMB$_{LxVMut}$	159 ± 30	158± 30	103 ± 9	73.2 ± 6.4
CLMB$_{WT}$	267 ± 21	265 ± 21	585 ± 57	426 ± 40

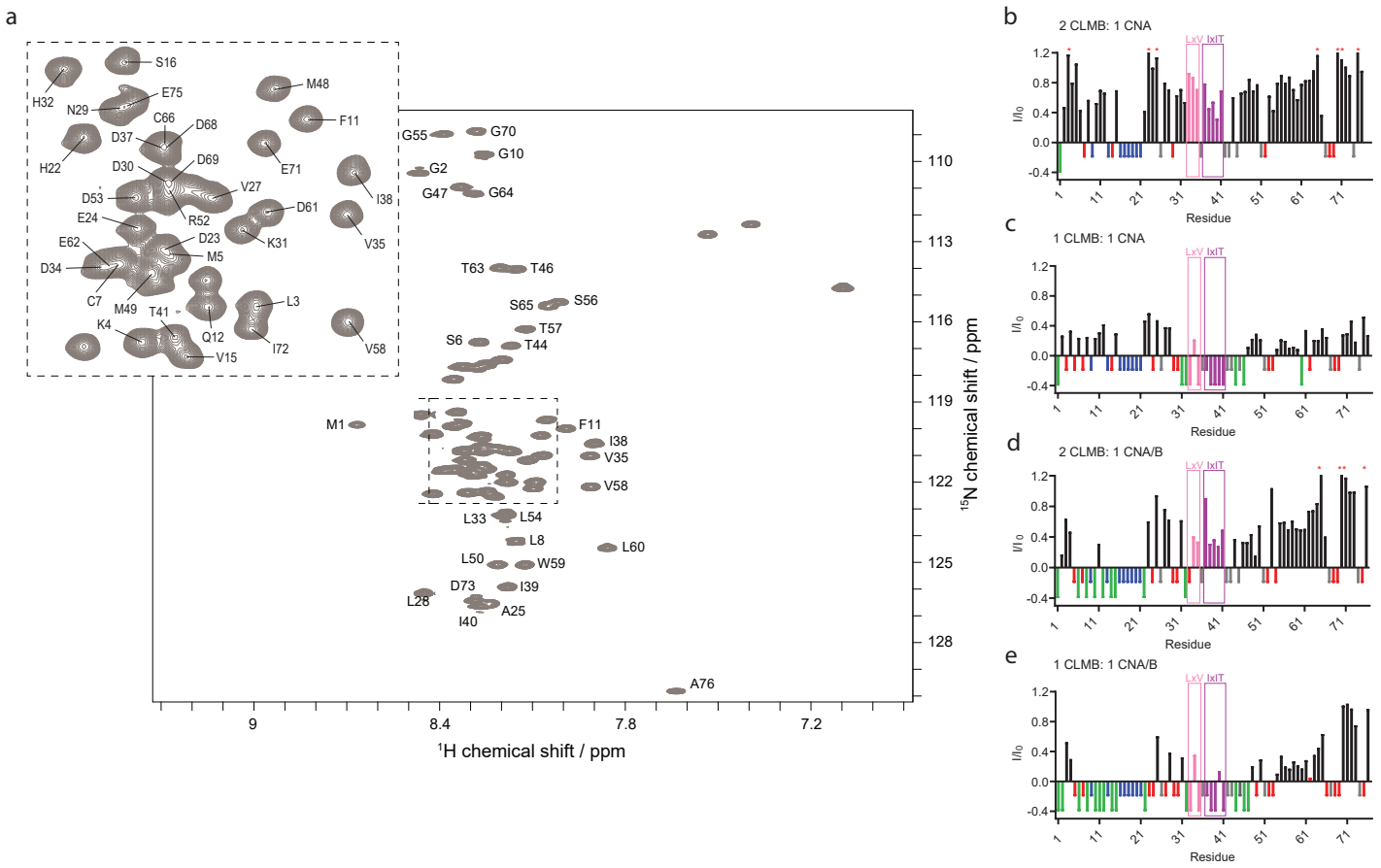
a
S16
H32
N29
E75
M48
F11
C66
D68
D37
H22
D30
D69
E71
I38
D53
V27
D61
E24
R52
K31
V35
E62
D23
M5
D34
C7
M49
T41
L3
K4
Q12
I72
V58
V15
G55
G70
G10
G2
G47
G64
T63
T46
S65
S56
T57
S6
T44
M1
F11
I38
V35
V58
L33
L54
L8
L60
L50
W59
D73
I39
L28
A25
I40
A76
110
113
116
119
122
125
128
9
8.4
7.8
7.2
^{1}H chemical shift / ppm
^{15}N chemical shift / ppm
b
2 CLMB: 1 CNA
c
1 CLMB: 1 CNA
d
2 CLMB: 1 CNA/B
e
1 CLMB: 1 CNA/B
LxV
IxIT
I/I0
Residue

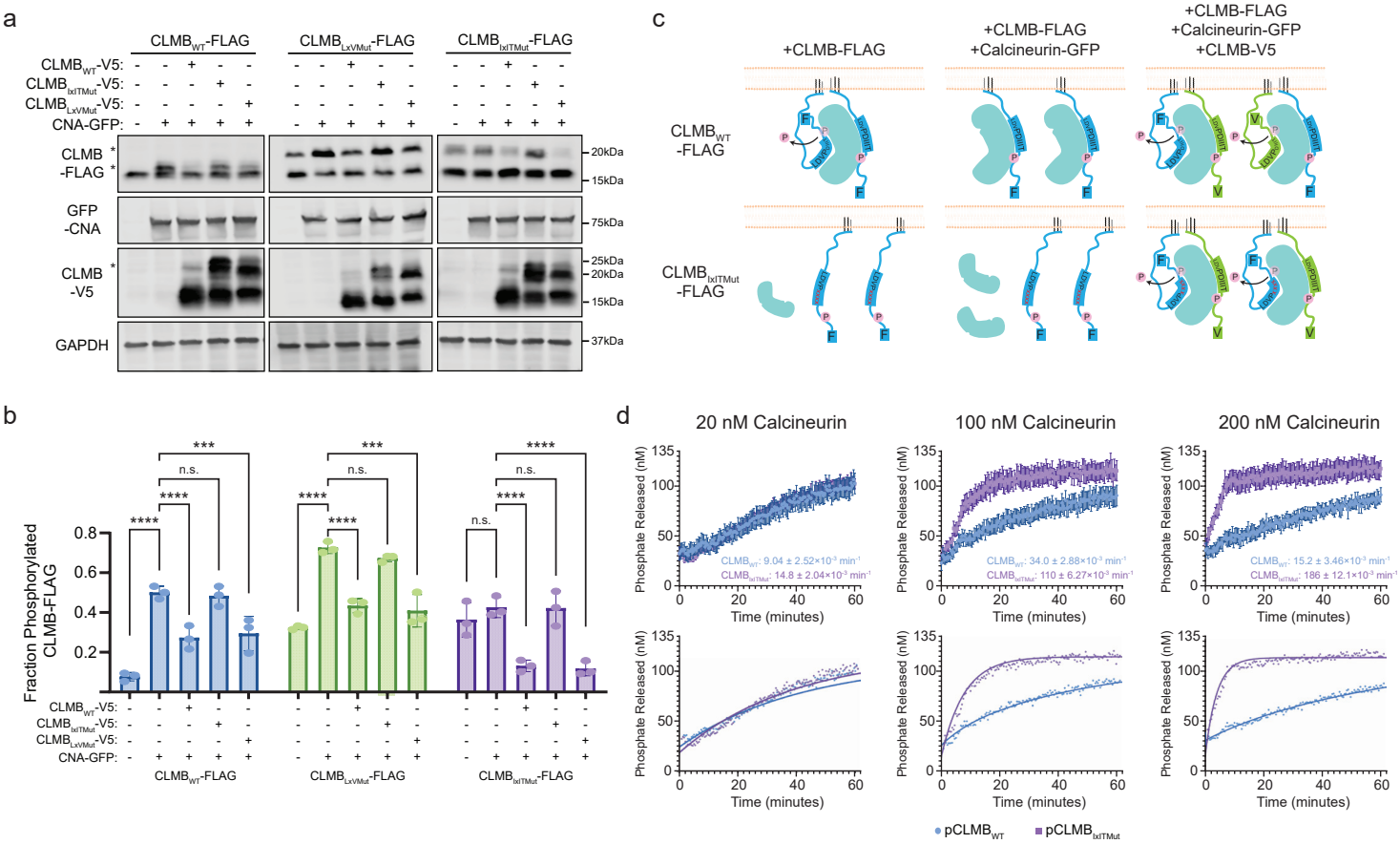
a
CLMB$_{WT}$-FLAG
CLMB$_{LxVMut}$-FLAG
CLMB$_{IxITMut}$-FLAG
CLMB$_{WT}$-V5:
CLMB$_{IxITMut}$-V5:
CLMB$_{LxVMut}$-V5:
CNA-GFP:
CLMB -FLAG
GFP -CNA
CLMB -V5
GAPDH
20kDa
15kDa
75kDa
25kDa
20kDa
15kDa
37kDa
b
Fraction Phosphorylated CLMB-FLAG
0.8
0.6
0.4
0.2
****
n.s.
***
CLMB$_{WT}$-FLAG
CLMB$_{LxVMut}$-FLAG
CLMB$_{IxITMut}$-FLAG
c
+CLMB-FLAG
+CLMB-FLAG +Calcineurin-GFP
+CLMB-FLAG +Calcineurin-GFP +CLMB-V5
CLMB$_{WT}$ -FLAG
CLMB$_{IxITMut}$ -FLAG
d
20 nM Calcineurin
100 nM Calcineurin
200 nM Calcineurin
Phosphate Released (nM)
Time (minutes)
CLMB$_{WT}$: 9.04 ± 2.52×10^{-3} min^{-1}
CLMB$_{IxITMut}$: 14.8 ± 2.04×10^{-3} min^{-1}
CLMB$_{WT}$: 34.0 ± 2.88×10^{-3} min^{-1}
CLMB$_{IxITMut}$: 110 ± 6.27×10^{-3} min^{-1}
CLMB$_{WT}$: 15.2 ± 3.46×10^{-3} min^{-1}
CLMB$_{IxITMut}$: 186 ± 12.1×10^{-3} min^{-1}
pCLMB$_{WT}$
pCLMB$_{IxITMut}$

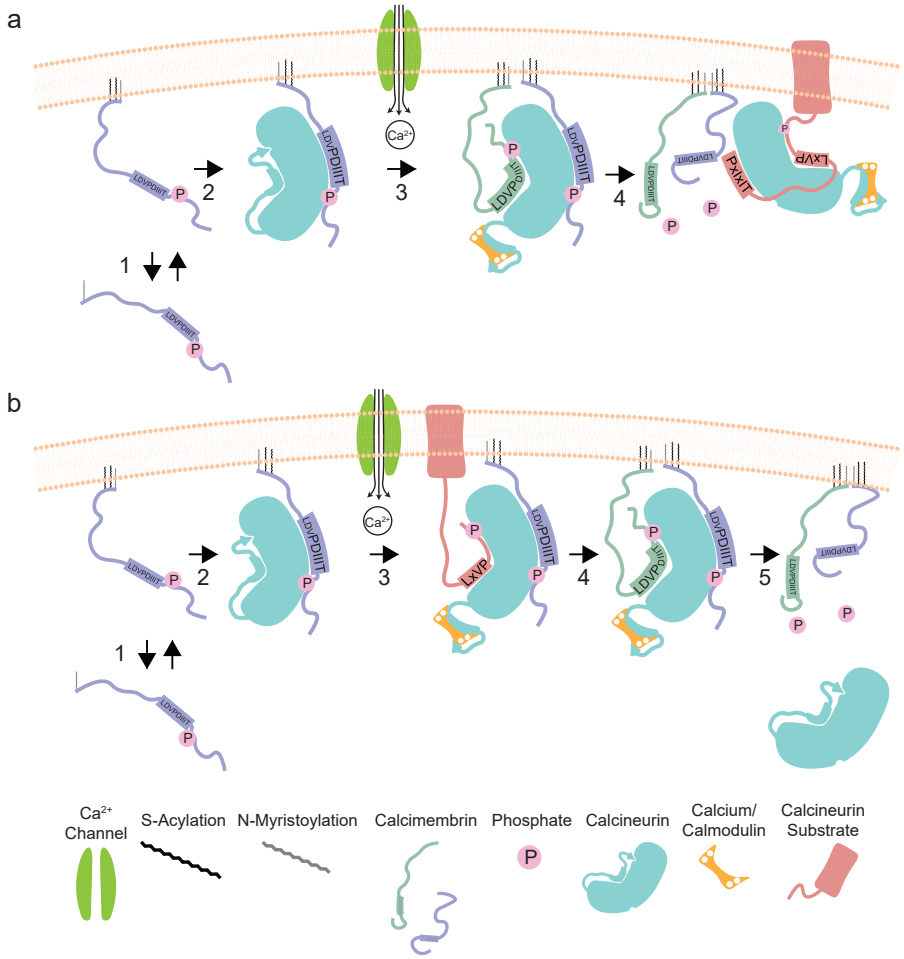
a
b
Ca2+
LDVPDIIIT
LDVPDIIIT
PxxIIT
LxVP
LxVP
P
1
2
3
4
5
Ca2+ Channel
S-Acylation
N-Myristoylation
Calcimembrin
Phosphate
Calcineurin
Calcium/ Calmodulin
Calcineurin Substrate